Chirality and Semiconducting-Enriched Single-Walled Carbon Nanotubes and their Applications in Chemical Sensing and Memory Devices

by

Michael Chido

B. A. in Chemistry, The College of Wooster, 2013

Submitted to the Graduate Faculty of the

Kenneth P. Dietrich School of Arts and Sciences in partial fulfillment

of the requirements for the degree of

Master of Science in Chemistry

University of Pittsburgh

2017

UNIVERSITY OF PITTSBURGH

DIETRICH SCHOOL OF ARTS AND SCIENCES

This thesis was presented

by

Michael Chido

It was defended on

December 6, 2017

and approved by

Shigeru Amemiya, PhD, Professor

Haitao Liu, PhD, Associate Professor

Thesis Director: Alexander Star, PhD, Professor

ABSTRACT

Chirality and Semiconducting-Enriched Single-Walled Carbon Nanotubes and their Applications in Chemical Sensing and Memory Devices

Michael Chido, M.S.

University of Pittsburgh, 2017

Single-walled carbon nanotubes (SWCNTs) have shown true promise as highly sensitive chemical sensors and high-performance electronic devices. Only recently, methods have been developed to further purify and separate nanotubes by their electronic properties, metallic or semiconducting, and even by type as individual chiralities. These developments have opened up possibilities to further improve and understand the properties of SWCNTs on a fundamental level. In this work, the exquisite properties of chirality-enriched and semiconducting-enriched SWCNTs (s-SWCNTs) have been explored for applications as chemical sensors and memory storage devices. In the first project, column chromatography was used to separate and enrich specific SWNCT chiralities. Using the product from this process, it was found that the sensor response of chirality-enriched (7,5) SWCNT field-effect transistors (FETs) to monosubstituted benzenes show a linear relationship with the Hammett parameter of the species tested, as was previously found for SWCNT mixtures. In a second project, we explored the properties of poly(oxacyclobutane) (POCB) and its crystallization with water at room temperature to form a polymer hydrate crystal structure. This polycrystalline material was found to have aligned 1D columns of water contained within its structure and we found that the material can be capacitively charged. The crystallization of the polymer and water was observed with electronic measurement by s-SWCNT FET devices as a large increase in capacitance was observed upon crystallization. These POCB-coated s-SWCNT devices were applied as memory cell devices and

showed bit separation of 10^4. In the final project, metal nanoparticle decorated s-SWCNT devices were applied as gas sensors in a proof of concept experiment using the AC heterodyne measurement technique. We showed that even in the presence of large charge transfer, such as hydrogen binding to palladium nanoparticles on the surface of SWCNTs, there is no signal with the AC method as opposed to the large signal observed in traditional DC FET measurement. Hydrogen sulfide elicited a sensor response in both AC and DC techniques as was expected.

TABLE OF CONTENTS

LIST OF FIGURES

Preface

This is dedicated to my family and friends that supported me throughout the many years of my education leading up to this Master's Thesis. This long journey and the experiences associated with it have made me grow into my own as a scientist. Without your support and encouragement for me to always do my best, I would not be where I am today and I am forever grateful.

1.0 INTRODUCTION

Since the recognition of carbon nanotubes as a new carbon allotrope,[1] scientists have sought to exploit their electrical and chemical properties. Nano-electronics based on carbon nanotube transistors have revolutionized the field of chemical sensors and have spurred interest in high performance carbon nanotube transistors for integration into consumer electronics. Since the first reported carbon nanotube transistor operating in ambient conditions,[2] publications based on carbon nanotube based transistors have become very prolific in the literature (Figure 1).

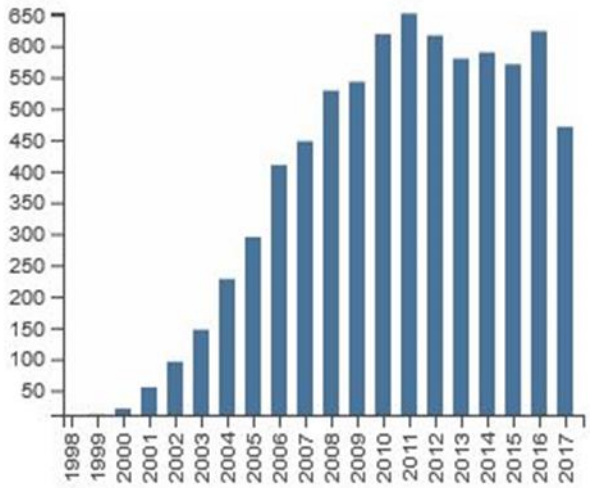

Figure 1. Publications on "carbon nanotube transistor" research since the first implementation in 1998 gathered from Web of Knowledge (accessed Nov. 7, 2017)

Interest in carbon nanotube transistors peaked around 2011 and since has been on a steady decline (based on publications in the field). The story of carbon nanotube hype and decline was even the cover story for Chemical and Engineering News in June 2015.[3] Many of the

"low hanging fruits" for carbon nanotube transistor research as chemical sensors and electronic devices have already been published. Within the past few years, highly purified and highly semiconductor-enriched carbon nanotubes have become commercially available. Though single isolated carbon nanotube species are not yet available in the market, experimental methods have been developed to separate nanotubes by type.

There has been a drive in the research community to develop and optimize single-walled carbon nanotube (SWCNT) separations. As-synthesized SWCNTs statistically contain about one-third metallic nanotubes. The presence of these metallic entities decreases the performance of carbon nanotube field-effect transistors (CNT FETs), so there is much interest in using purified SWCNTs in these devices.[4-5] Having purified SWCNTs is vital for their integration into high performance logic circuits, development of highly sensitive chemical sensors, and fundamental electronic studies of carbon nanomaterials. Finding scalable and cost-effective separation techniques is key to making these separated SWCNTs available to the greater scientific community. The focus of carbon nanotube sensor research has been based on field-effect transistor devices. An ideal transistor has an active channel made up of a purely semiconducting material which allows for low power and high gain devices. The current gold standard transistor material is doped silicon and advances with development of this material has led to the miniaturization and ubiquity of high performance silicon-based computers. SWCNTs have the potential to outperform silicon in theory and very convincing small-scale demonstrations have been demonstrated recently.[6] Computer companies have also been investing in methods of large-scale assembly of SWCNT transistors for computing applications.[7]

There are two main types of carbon nanotubes used in this research which are defined by their characteristic diameter range. Arc discharge (AD) nanotubes are produced from high

voltage arc discharge of graphite electrodes.[1] Due to the high temperatures that result at the anode in this setup, carbon nanotubes are produced. AD-produced nanotubes are readily available and can be purchased in highly purified forms without residual metal catalyst and usually form large diameter SWCNTs (average 1.4 nm diameter). Semiconducting-enriched SWCNT (s-SWCNT) inks are commercially available and used throughout this work. Another type of SWCNTs, high pressure carbon monoxide (HiPCO) are produced in a chemical vapor deposition (CVD) setup. In the HiPCO process, catalytic iron clusters are produced by condensing iron penta-carbonyl onto a substrate. These nucleated clusters are then exposed to a flow of carbon monoxide gas at very high pressures (30-50 atm) and high temperatures (900-1100°C) which decomposes and grows well defined, pristine carbon nanotubes on nucleated iron clusters.[8] This process forms smaller diameter nanotubes with an average of 1.0 nm diameter.

Future research in the field of carbon nanotube transistors will depend upon very pure, type-separated nanotube devices to understand the fundamental interactions that give rise to carbon nanotube FET sensing and desirable electronic properties to make the improvements necessary to bring SWCNT devices to the forefront of consumer devices.

1.1 CARBON NANOMATERIALS

Though the actual definition of a “nanomaterial” can be quite vague, a widely accepted definition is that a nanomaterial must at least have one dimension between 1-100 nanometers. These materials can’t be observed by traditional optical methods due to the resolution of these methods being dependent on the wavelength of visible light. Nanoscience has become a very well-established field, mostly due to advances in electron microscopy in the past few decades

and synthesis and characterization of nanomaterials with these advanced tools. Nanomaterials have garnered interest due to the interesting properties that arise from their small size. Due to quantum confinement effects, classical mechanical models fail to describe the properties of nanomaterials. Instead, quantum mechanics must be applied to explain nanomaterial properties. The fundamental limits for many types of carbon nanomaterials have shown some very promising possibilities and is the motivation for much of the work in the field.

There are three main types of carbon nanomaterials, which are defined by how many dimensions of the material are "nano," or small enough to be modeled by quantum mechanics. When one dimension of a material is nano-sized, that dimension is not considered when describing its dimensionality. For example, if a material only has one dimension in the nano regime, it is called 2D. The 0D carbon nanomaterial, fullerene, was the first of the carbon nanomaterials to be discovered (Figure 2, left).[9] Fullerenes are closed cages of sp^2 hybridized carbon which include discrete numbers of carbon atoms. This was followed by the discovery 1D carbon, the carbon nanotube (Figure 2, center).[1] Though the focus of this study will be on single-walled carbon nanotubes (SWCNTs), it should be noted that other carbon nanotube categories also exist. Double-walled nanotubes[10] exist as a SWCNT inside of a larger diameter SWCNT. Multi-walled carbon nanotubes can include many nanotubes all encapsulated in multiple layers of procedurally larger nanotubes. 2D carbon was later isolated and given the name graphene.[11] Graphene is a single layer, flat sheet of sp^2 hybridized carbon (Figure 2, top). When a carbon nanomaterial is mostly comprised of carbon in the absence of oxygen defects, the material is called "pristine."

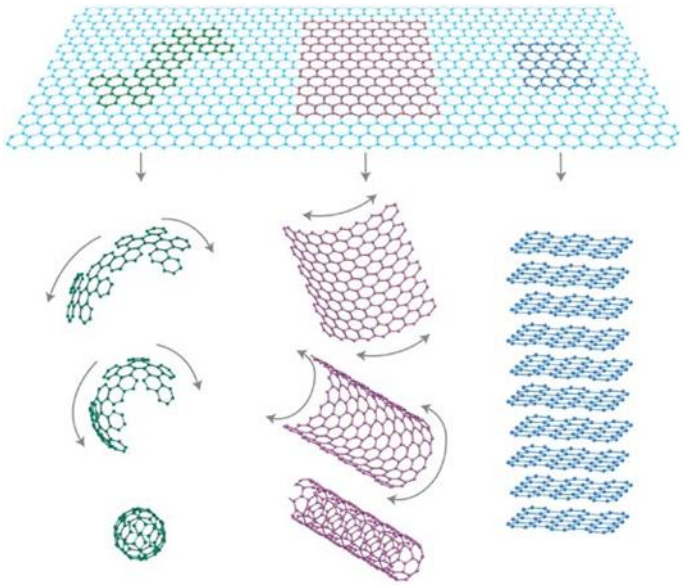

Figure 2. Fullerenes (left), carbon nanotubes (middle) and graphite (right) in relation to graphene (top). These three allotropes of carbon make up the field of carbon nanotechnology. Reprinted by permission from MacMillan Publishers Ltd: Nature Materials ref [12], Copyright 2007.

Carbon nanotubes can be visualized as rolled up sheets of graphene,[13] and the roll vector indicates the type of nanotube. The shape of a carbon nanotube is cylindrical, but different roll vectors will produce a twist in the structure.[13] One can construct different carbon nanotube species, or chiralities, of carbon nanotubes by using the honeycomb lattice of graphene as a base and tracing out two vectors to indicate the circumference of the structure (Figure 3). These vectors are called "chiral indices" and two chiral indices combined describe the total chiral vector (C_h) described in Equation 1.

$$C_h = n * a_1 + m * a_2 \quad (1)$$

Where a_1 and a_2 are the chiral indices and both "n" and "m" are integers greater than 0. The chiral vector is then expressed as (m, n). The diameter of the nanotube can then be derived by using the lattice constant (a = 0.249 nm) of a honeycomb lattice of sp^2 carbon.

$$d_t = \frac{a}{\pi}\sqrt{n^2 + m^2 + nm} \quad (2)$$

The chiral vector, and therefore the diameter, determines the properties of the carbon nanotube species of interest. Two achiral types of nanotubes result from m = 0 and n = m, namely zigzag and armchair, respectively. All other combinations of chiral indices result in what is called a chiral nanotube.[13] SWCNTs typically have diameters of 0.8 – 2 nm and lengths can vary dramatically. SWCNTs from tens of nm[14] to nearly four centimeters[15] have been synthesized. Generally, SWCNTs as purchased have a length on the micron scale and these lengths are shortened by solution processing during sonication.

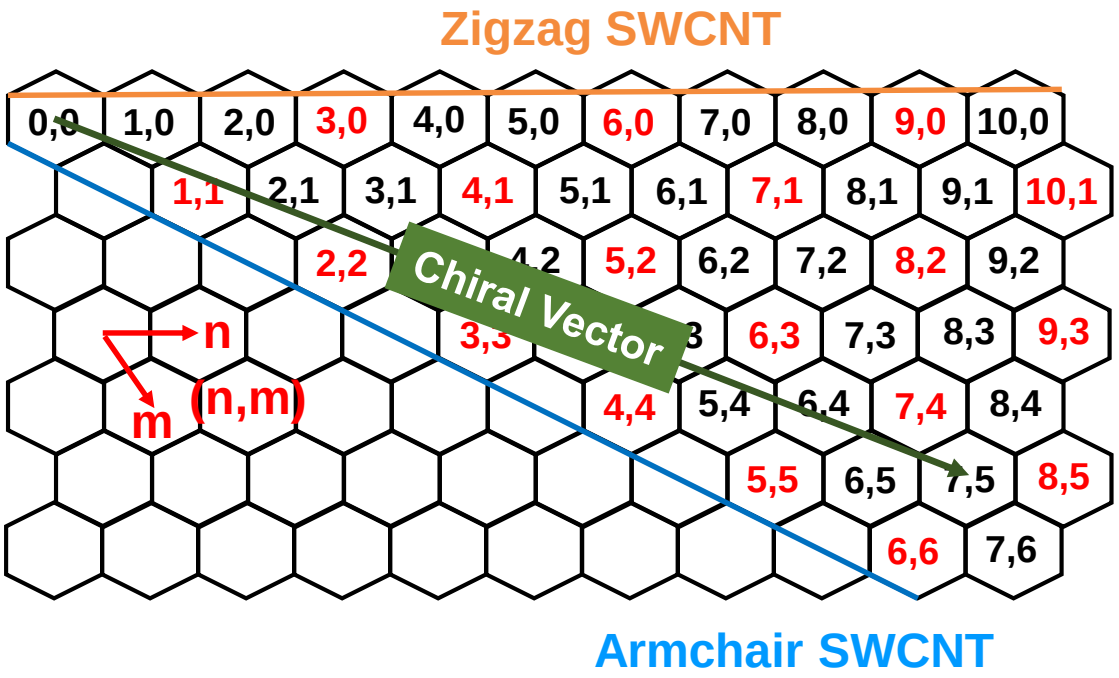

Figure 3. Diagram illustrating the convention for chiral index labeling of SWCNTs. The chiral vector makes up the circumference of the nanotube. Chiral indices in red represent metallic nanotubes, while others are semiconducting.

One very interesting result of quantum confinement effects in carbon nanotubes is that a nanotube's metallicity is directly affected by the chiral angle of the carbon nanotube. Theory predicts that metallic nanotubes will result from chiralities in which n – m = 3*k, where "k" is an integer value. Semiconducting nanotubes result from chiral indices where n – m is not equal to 3

multiplied by an integer.[13] Examples of this differentiation of carbon nanotube metallicity are illustrated in Figure 3.

1.2 SPECTROSCOPY OF CARBON NANOTUBES

Since the discovery of carbon nanotubes, their electrical properties have been very thoroughly investigated. For these types of investigations, SWCNTs are the main focus due to their electrical properties, photoluminescence, absorbance, and the potential for purification of individual chiral species.[16-17] SWCNTs can be investigated by optical spectroscopies due to Van Hove singularities[18] in the density of states which lead to discrete electronic transitions dependent on the diameter of the SWCNTs. These transitions are referred to in a shorthand notation indicating the Van Hove transition and the metallic or semiconducting nature of the nanotube of interest. For example, a metallic nanotube transition between the first Van Hove singularities above and below the Fermi level would be referred to as an M_{11} transition. The letter (M or S) refers to a metallic or semiconducting nanotube and the numbers correspond to the Van Hove singularities above and below the Fermi level which describe the electronic transition (Figure 4).[19]

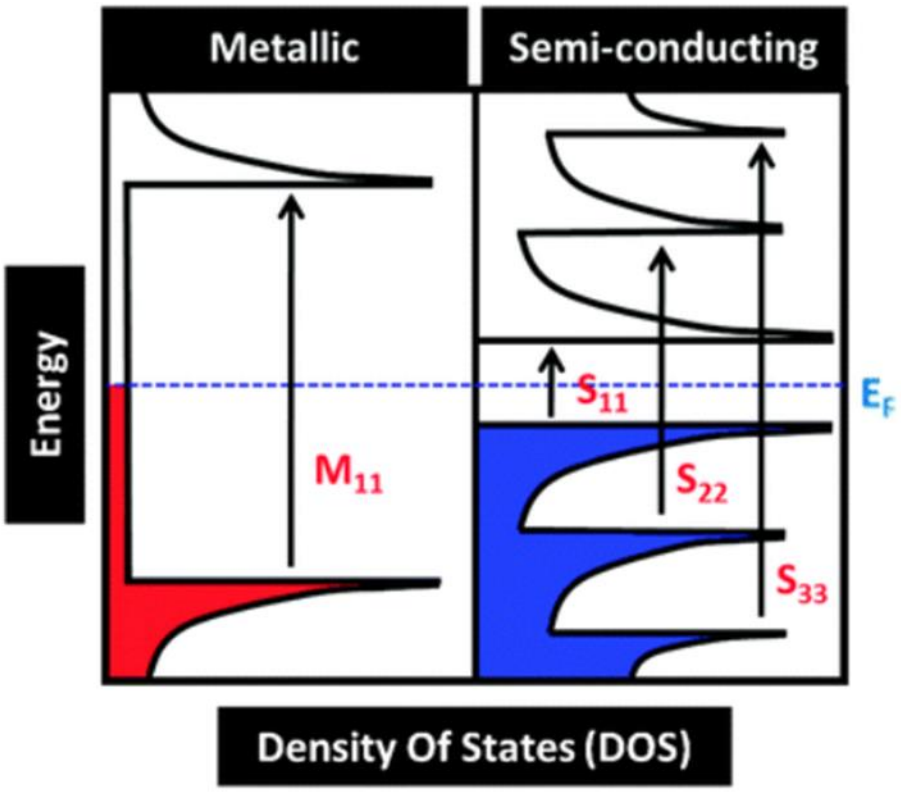

Figure 4. Van Hove singularity allowed transitions illustrated for metallic (left) and semiconducting (right) carbon nanotubes. The Fermi level (E_f) is shown in dashed blue. Reproduced from ref [19] with permission of The Royal Society of Chemistry.

The most common forms of spectroscopic characterization of SWCNT samples are Raman spectroscopy,[20-21] UV-vis-NIR absorption spectroscopy,[22] and photoluminescence spectroscopy.[23] The band gap energies of nanotube chiralities have been empirically investigated in terms of absorption energies[22] as well as excitation/emission photoluminescence measurements.[23] Raman spectroscopy was used to complement these initial studies to confirm chiral index assignments. Raman spectroscopy can also be used to investigate diameter-dependent radial breathing modes in carbon nanotube samples. This method is not commonly used to analyze chirality content in bulk samples due to the strong dependence of different SWCNT chiralities on the excitation energy, leading to resonance conditions determining the

nanotubes which are shown in the spectrum.[20] Raman spectroscopy is also very commonly used to test the level of defect density of carbon nanomaterials.

1.2.1 UV-vis NIR Absorption Spectroscopy of SWCNTs

In a batch sample of SWCNTs, absorption spectra can be split into four regions of interest. The S_{33}, M_{11}, S_{22}, and S_{11} regions appear as broadened combinations of discrete van Hove transitions of all chiralities present in solution (Figure 5).

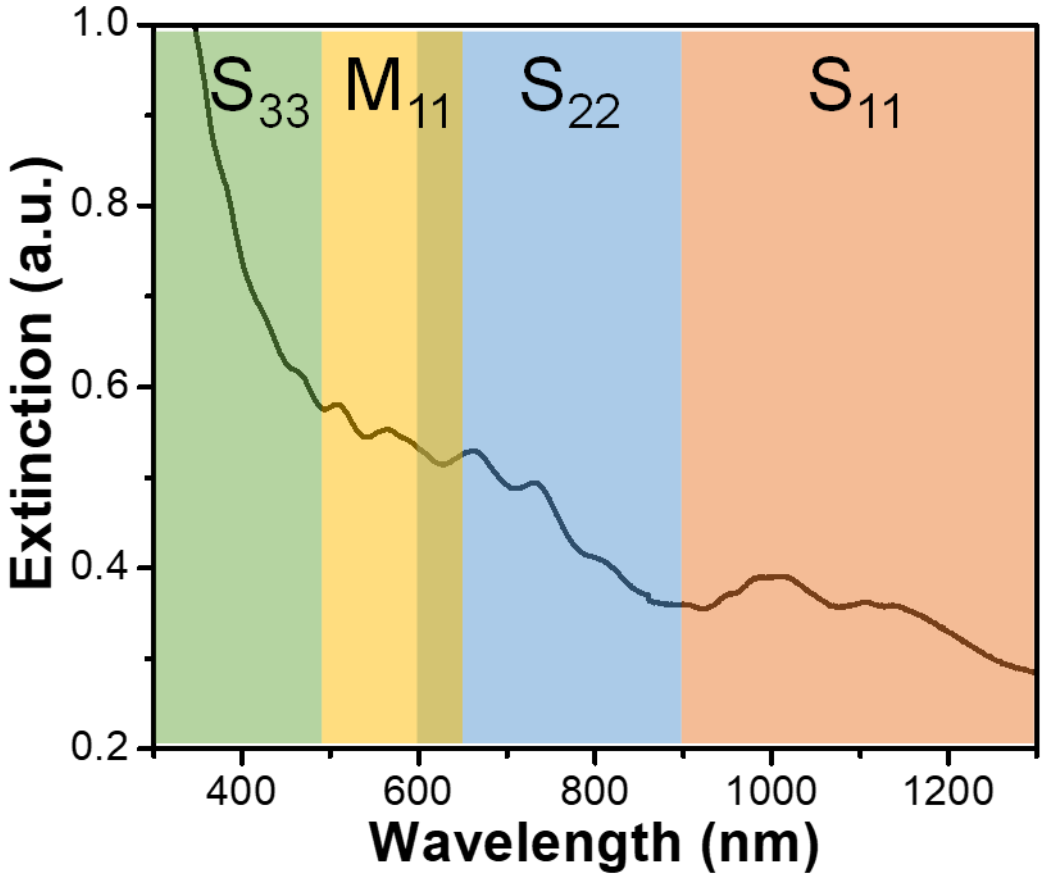

Figure 5. Typical absorption spectrum of a dispersed (2% SDS, water) solution of as-synthesized High Pressure Carbon Monoxide (HiPCO) SWCNTs. Van hove singularity energies for semiconducting and metallic SWCNTs are color-coded. The M_{11} and S_{22} regions have slight overlap.

UV-vis-NIR spectra can be used to determine the relative abundance of different chiral nanotube species in a bulk sample by careful deconvolution of raw data using known absorption wavelengths for relevant chiralities expected in the sample. Many publications have empirically assigned absorption energies to nanotube chiralities and this has led to empirical formulas which can be used to calculate the optical properties of carbon nanotubes based on their diameter.[24] The advantage of this type of analysis is that interrogation of the sample is fast and absorption spectroscopy instrumentation is ubiquitous in research institutions. Absorption spectroscopy also works for a wide range of SWCNT diameters including both HiPCO and AD nanotubes. There are a few disadvantages with this type of analysis as well: 1) Peak overlap can lead to difficulty in assignments resulting in sampling bias, 2) Chemical modification of SWCNT sidewalls can lead to peak maxima shifts, and 3) A large background is present due to scattering, resonance peaks, and pi-plasmon effects; and this leads to difficulty subtracting out the background which is necessary for peak fitting the data.[25] All of these effects can lead to error in analysis of chirality content in a SWCNT solution which cannot be easily quantified. To limit error, chirality content is assigned using the S_{11} transitions because they exhibit the least overlap of peaks compared with other transition regions.

1.2.2 Photoluminescence Spectroscopy of SWCNTs

Photoluminescence spectroscopy is a useful tool for qualitative bulk analysis of s-SWCNT chirality content. SWCNT fluorescence was first demonstrated by O'Connell *et al.*[26] Using fluorescence spectroscopy, one can construct a 2D contour map using excitation wavelength on the y-axis and emission wavelength on the x-axis. This is commonly referred to as an excitation-emission plot (or EE plot). The measurements are performed using visible light excitation (~400-

800 nm) and NIR emission detection. One of the limitations of these instruments is that they are generally more appropriate for small diameter SWCNTs found in HiPCO. To measure larger diameter SWCNTs, like those found in an AD sample, a special detector is necessary to measure the lower energy emission from these species. This method specifically investigates the S_{22} transition of the nanotubes as an excitation energy. The advantage with this technique is that there is little to no overlap of different chiral species in the spectrum and chirality assignments can be done with much more confidence than in absorption spectroscopy (Figure 6a) because of the extra dimension present in an E-E map. The drawback with this technique is that data acquisition takes much longer than simple absorption spectroscopy. Acquisition time is mainly limited by the detector used in the instrument, though modern fluorescence spectrometers will use a CCD detector for NIR emission which significantly decreases analysis time. SWCNTs must also be very well dispersed in solution to get good fluorescence as bundled nanotube fluorescence will be quenched.[27] Oxidized and highly defective SWCNTs also do not show fluorescence. This method does not give any information about metallic SWCNTs in the sample because metallic nanotubes do not fluoresce as the relaxation process happens thermally. Photoluminescence is not commonly used solely for chirality content analysis from separated nanotubes due to bundled SWCNTs not being addressed and many of these instruments are not equipped to measure the entire spectrum necessary to include all chiralities present in HiPCO. Generally, fluorescence will be coupled to other methods for secondary confirmation of findings. This can lead to discrepancies between chirality content calculated using UV-vis-NIR and EE mapping (Figure 6).

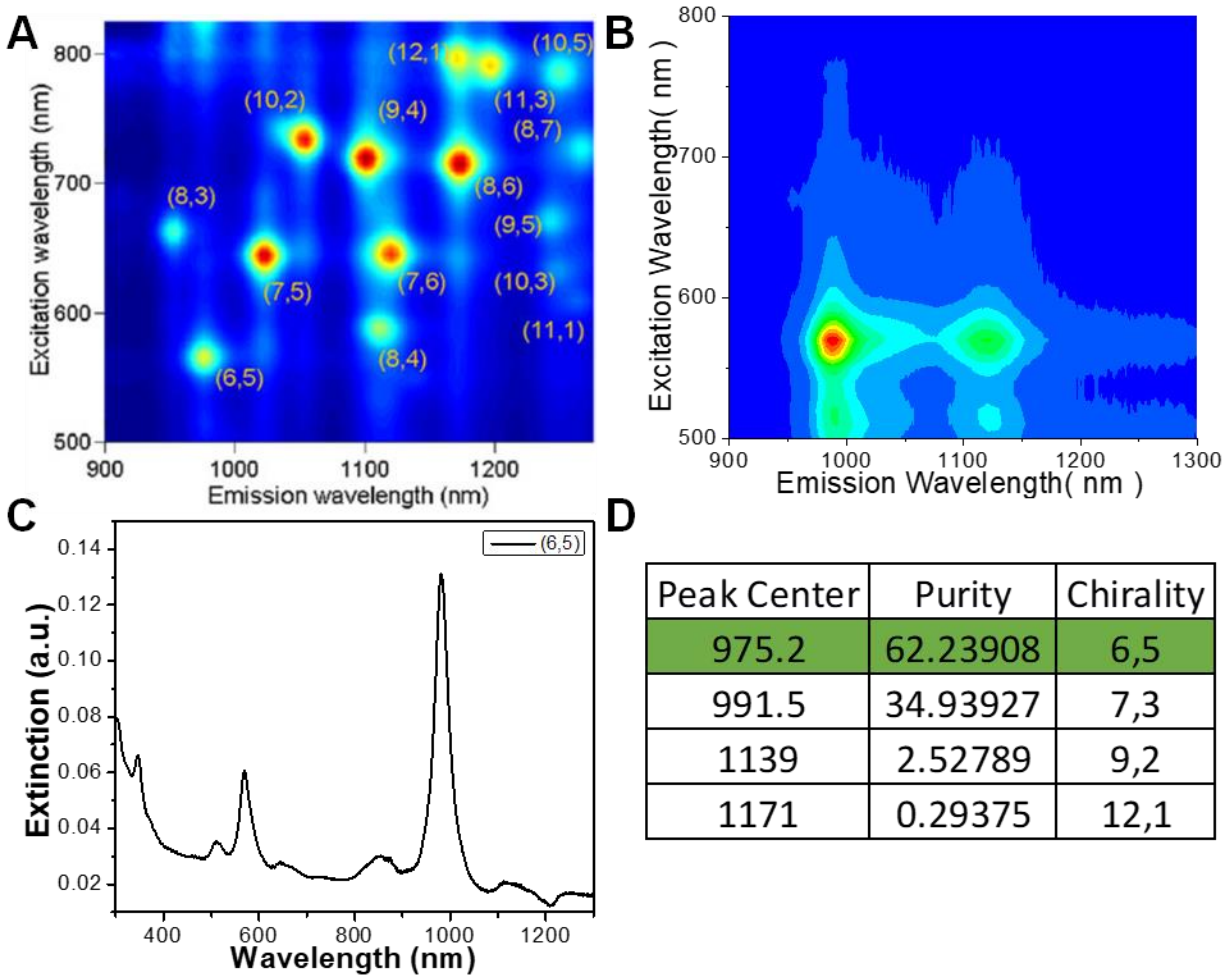

Peak Center	Purity	Chirality
975.2	62.23908	6,5
991.5	34.93927	7,3
1139	2.52789	9,2
1171	0.29375	12,1

Figure 6. Photoluminescence and absorption spectroscopy to calculate chiral abundance. A) PL EE map of stock HiPCO SWCNTs dispersed in SDS and water (adapted from [28]), B) PL EE map of chirality-enriched (6,5) SWCNT after column chromatography separation, C) Absorbance spectrum of the sample in "b", D) Calculated chiral abundances (purity) from data shown in "c" using peak fitting. Peak fitting very roughly agrees with the photoluminescence data. (7,3) and (9,2) would not appear in the PL EE map in the excitation range measured.

1.2.3 Raman Spectroscopy of SWCNTs

Raman spectroscopy has been widely used in the characterization of carbon nanotubes.[21-23, 29-31] This is due to the simplicity of the measurement and the wealth of structural information that can be obtained from the spectra generated. Information gathered from Raman spectra have been

used to identify the chiral index of individual SWCNTs based on their radial breathing mode (RBM) energies.[20] The regions of interest in the Raman spectra of SWCNTs are the RBM, D, G, and G' (resonance of G) peaks (Figure 7). The radial breathing mode is ultimately the result of radial expansion and contraction of the carbon atoms coherently out of plane.[29] The observed frequency of the RBM is generally between 100-500 wavenumbers (cm^{-1}) with the energy being inversely proportional to the diameter of the tube generally described in Equation 3 due to larger nanotubes containing more mass along the circumferential direction:

$$\omega_{RBM} = \frac{C}{d_t} \tag{3}$$

Where ω_{RBM} is the frequency observed in wavenumbers, C has units of cm^{-1}*nm and is empirically derived, and d_t is the diameter of the nanotube in nanometers. Different values of C are used and sometimes a correction term is added to account for substrate and tube/tube interactions.[23, 29]

The G peak in the Raman spectra of carbon nanotubes arises from in plane phonon modes between dissimilar carbon atoms in the unit cell of SWCNTs. The G band usually consists of two easily discernable components in large sample size of SWCNTs. The G- and G+ bands located at 1570 cm^{-1} and 1590 cm^{-1}, respectively. The G+ peak is associated with nanotube long-axis and is very sensitive to doping and charge transfer interactions. The G- peak arises from vibrations in the circumferential direction and the peak profile looks very different for metallic and semiconducting SWCNTs.[29, 32]

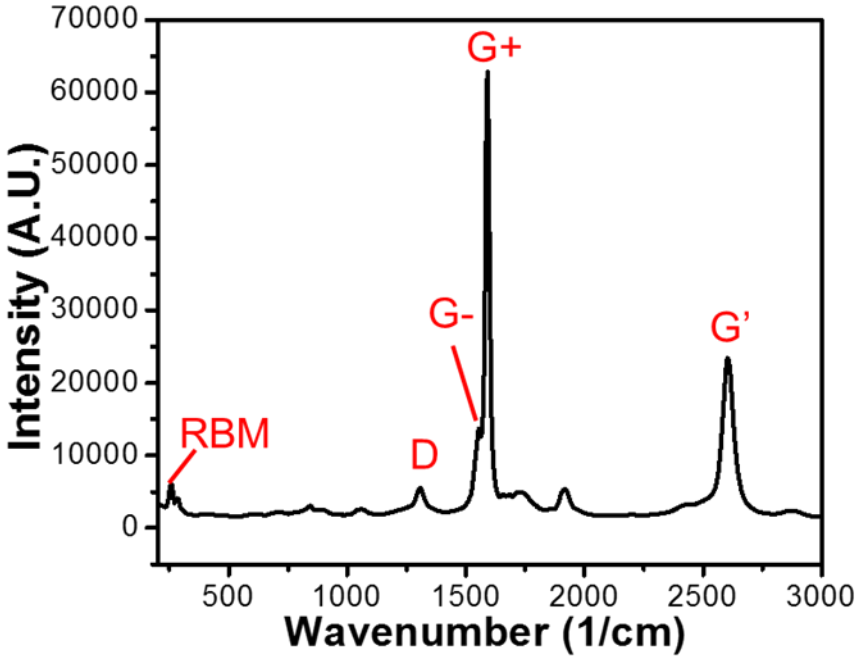

Figure 7. Typical Raman spectrum of a SWCNT sample on glass. Areas of interest in the Raman spectrum of SWCNTs are indicated.

The D and G' peaks can both be used to probe structural modifications to the sidewalls of SWCNTs. These can either be intentional modifications or defect sites which give rise to a shift in G'[32] and increase in D peak intensity. A common use of the D peak is comparing its integrated area with the area of the G peak, referred to as the D/G ratio. One can get a rough estimation of the purity of SWCNT samples by utilizing this method where a low D/G would indicate more pure, pristine material.[29]

1.3 SINGLE-WALLED CARBON NANOTUBE SEPARATIONS

Carbon nanotube separations have been developed for metal/semiconductor separations as well as single-chirality isolation. There are two general schemes for SWCNT purification and isolation, bottom up approaches and post-synthesis separations. Recent work has begun

developing bottom-up synthesis of diameter controlled s-SWCNTs utilizing high melting point tungsten alloy nanoparticles of well-defined diameters in CVD growth conditions.[33-34] Research has also shown that SWCNTs can be "cloned" from pre-existing single chiral tubes by epitaxial growth mechanisms by using the nanotube as a growth seed.[35-36] This method requires that you start with single chiral SWNCT samples and yield is relatively low.

The focus of the presented work will be on post-synthesis purification methods. This is due to the possibility of scaling up separations and very pure, high quality SWCNTs are commercially available. The first SWCNT separations were developed to separate s-SWCNTs or m-SWCNTs from as-synthesized batches of SWCNTs. Density gradient ultracentrifugation[37-39] and column chromatography[17, 40] have both been used to isolate s-SWCNTs either as mixtures or single-chiral products. Polymer based extraction methods have been used for the separation of s-SWCNTs from mixtures by utilizing selective wrapping of polymers on s-SWCNT species.[41-43] Polymer-based extraction has led to the commercialization of 99% and higher enriched s-SWCNTs due to the simplicity and scalability of polymer-based methods. Refinement of the many chiralities of s-SWCNTs still requires iterative column chromatography and while these methods are well understood in the literature, single chiral species are not commercially available due to difficulty with scaling up these processes.

1.3.1 Column Chromatography

Column chromatography separations of SWCNTs are cost effective, scalable, and do not require complex or expensive instrumentation. The first very successful single-chiral SWCNT separation utilizing column chromatography was demonstrated by Kataura's group in 2011.[17] This paper garnered much interest in the field of column chromatography separations of SWCNTs.

Many of the publications following this breakthrough in 2011 sought to optimize the separation method for more efficient separations through an understanding of the mechanism behind SWCNT separation by column chromatography (Figure 8A).[44-46] The most commonly used gel in these separations is Sephacryl S200 (GE Healthcare Life Sciences). This material is a hydrophilic cross-linked copolymer of allyl dextran and N,N'-methylene bisacrylamide with varying pore sizes dependent on the degree of cross-linking in the polymer. Though this method was initially considered a form of size-exclusion chromatography due to the ability to separate based on diameter, researchers came to realize that the pore size of Sephacryl S200 was not small enough to allow for differentiation between these ~1 nanometer-sized diameter dimensions of HiPCO SWCNTs by the traditional size-selective pore mechanism.

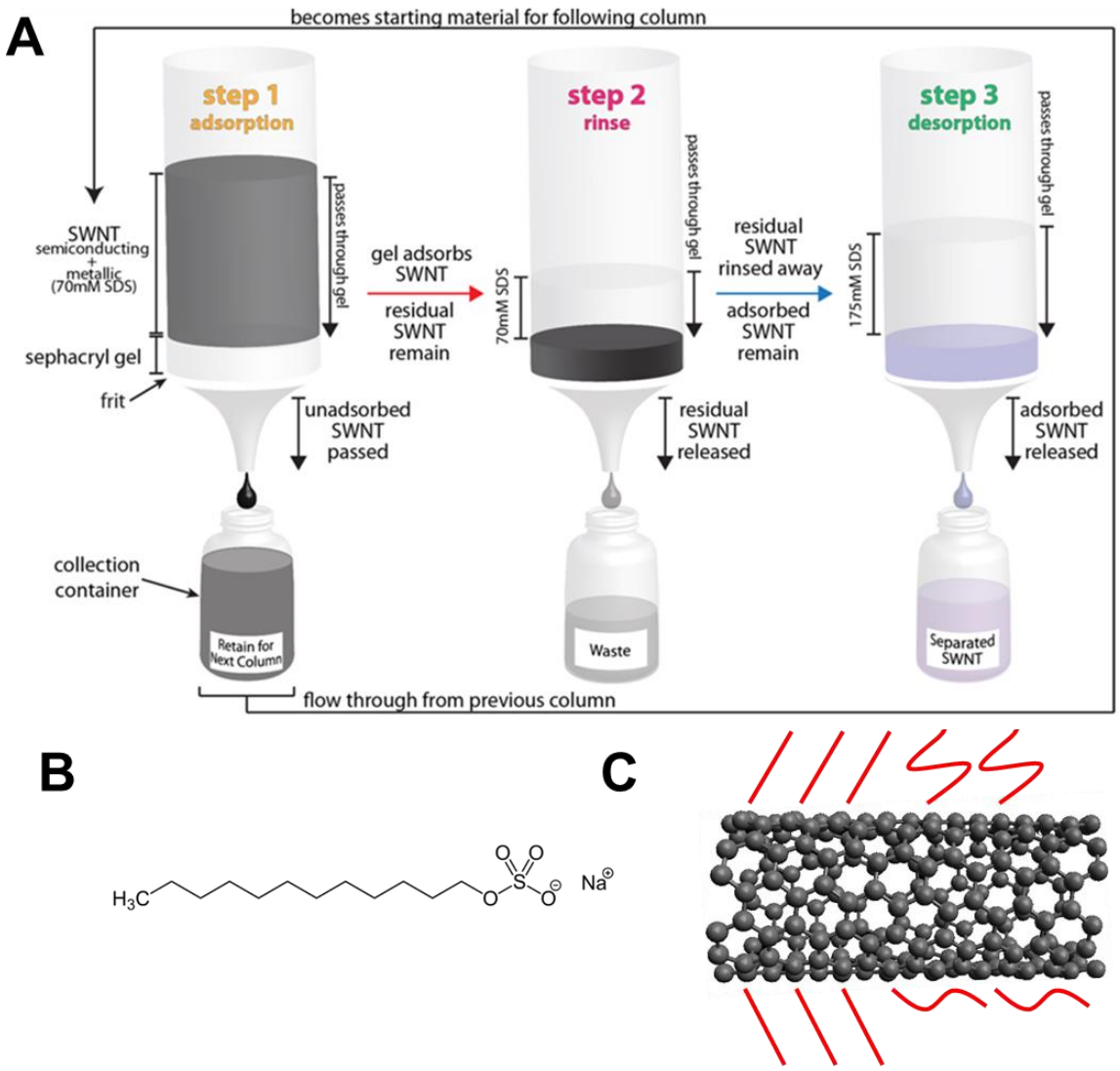

Figure 8. SWCNT chirality enrichment procedure. A) General outline of column chromatography separation procedure of SWCNTs. Reprinted with permission from [40]. Copyright 2013 American Chemical Society. B) Structure of sodium dodecyl sulfate (SDS). C) Cartoon of SDS adsorption on a (7,5) SWCNT illustrating regions of close, tight packing and defective regions dependent on the chiral angle.

Sodium dodecyl sulfate (SDS) (Figure 8B), commonly used in these separations as a surfactant for the SWCNTs, is known to adopt different self-assembled structures on nanotube surfaces dependent on the curvature (Figure 8C).[47] Changes in charged head-group packing as well as counter-ion residence times lead to very different local environments directly dependent on the curvature of SWCNTs. Initially, it was shown that changes in the permanent dipole

moment of agarose gels drastically reduce the retention of SDS-wrapped SWCNTs on agarose columns. This lead to the idea that the separation occurs due to ion-dipole interactions between SDS-SWCNTs and the column media, respectively. This study directly addresses the large differences in adsorption of metallic and semiconducting SWCNTs in column separations by treating the nanotubes as macro-ions and relating their adsorption strength to their polarizability.[44] Utilizing a kinetic binding model for different chiralities in Sephacryl separations,[40] Strano and co-workers evaluated short-range and long-range interactions between SWCNTs and Sephacryl medium. They found that long-range electrostatic repulsion forces were mostly responsible for differences in binding of chiralities. These forces are directly due to the conformation and packing density of SDS on SWCNTs leading to differences in electrostatic repulsion of individual chiral species.[46] This electrostatic interaction is most likely between the SDS-SWCNT and hydroxyl groups on the gel medium which was determined by comparing dextran-based gel (Sephacryl) with agarose gels for the separation of SWCNTs. They found that increased dextran content in the Sephacryl gels lead to considerably higher retention of SWNCTs and chiral selectivity in the columns. Interestingly, agarose column chromatography can yield very high purity (~98%) metallic nanotubes with low throughput while dextran-based media separate semiconducting nanotubes in a higher throughput manner. Dextran-based gel media cannot be used multiple times for a SWCNT separation, which is a major downfall of the material.[45]

1.3.2 Density Gradient Ultracentrifugation

Density gradient ultracentrifugation (DGU) is a form a differential centrifugal purification which separates targets by minor differences in isopycnic point (buoyant density). DGU is usually

performed by applying the sample to be separated to a preformed viscous solution with a gradient of density as a function of centrifuge tube depth. At the very bottom of the tube, density is highest and this density decreases closer to the top of the tube. In an ultracentrifuge, the components of the sample to be purified will diffuse through the gradient medium until they match the isopycnic point of the surrounding medium. The separation of species based on buoyant density results in bands at different regions of the tube which can then be fractionated out to isolate different species. DGU was initially applied to SWCNTs for separation based on chirality in 2005.[39] This work showed that density gradients based on iodixanol were capable of separating SWCNTs by diameter after ultracentrifugation. Hersam and co-workers found that smaller diameter SWCNTs were more buoyant than large diameter tubes and this difference was enough to be a pronounced separation in the conditions tested.[39] DGU was later optimized to get more band separation based on nanotube diameter in a very influential Nature Nanotechnology paper.[16] Hersam and co-workers found that the surfactant used to solubilize the nanotubes plays a major role in the separation by directly affecting the buoyant density of the nanotube species. In this case, they found sodium cholate to be an optimal surfactant for efficient separation. This form of separation requires a preparative scale ultracentrifuge, which is not readily available to many and also represents a very large energy input required for separation.

1.3.3 Polymer-Based Extraction Methods

Polymer-based extraction methods have been developed as an alternative method for separating SWCNTs by type (metallic vs. semiconducting) with less focus on separating each single chiral species. The first observation of chirality-dependent polymer wrapping around SWCNTs occurred in 2007.[41] In this work, the authors observed that by adding certain polymers to

solutions of SWCNTs, there appeared to be selective wrapping of the polymers around the SWCNTs based on polymer rigidity as well as the chiral angle and diameter of the SWCNTs.[41] This initial observation initiated the field of polymer-based SWCNT separations based on selective wrapping and solubility dependent on chiral angle. Many different types of polymers have been synthesized and tested with varying amounts of success. It was discovered that polyfluorene-based polymers with alkane pendant groups (octyl) work well to selectively wrap and suspend semiconducting SWCNT species.[43] Though polyfluorene with octyl groups (PFO) worked well to suspend semiconducting, small diameter SWCNTs, there was a need to extend this selectivity to large diameter SWCNTs as these are more desirable for electronic devices.[48] Optimization of the polyfluorene method led to utilization of poly(9,9-di-*n*-dodceylfluorene (aka. PFDD) for large diameter SWCNTs.[49] The s-SWCNT inks used in some of the following projects (called "Isosol S100") were extracted utilizing the PFDD method.

1.4 FIELD-EFFECT TRANSISTORS

The field-effect transistor effect was first discovered by Julius Edgar Lilienfeld in 1926,[50] though this effect was not explained or put into practical use until ~20 years later by William Shockley, Walter Brattain, and John Bardeen working at Bell Labs. These three scientists were awarded the Nobel Prize in Physics in 1956 for the discovery of the transistor effect and its application. Transistors have been largely responsible for the implementation of the personal computer, a major milestone of technological progress. Transistor miniaturization continues to be at the very forefront of technological advance in computer processors with continual improvements of speed and efficiency being a result.

The general concept underlying the field-effect transistor effect is that a semiconducting material's resistance to current flow can increased or decreased by influencing majority or minority carriers (holes and electrons) through use of a "gate" electrode. This effect allows one to control the transistor as a voltage controlled switch. A semiconducting material is contacted with source and drain electrodes and a gate electrode is used to influence the conducting channel in the material by pinching the conductive channel closed or forcing it open. The open and closed states of the channel result in two absolute electrical states of a transistor, on and off (a transition state between the two absolutes exists as well) which can be influenced by an electrical signal from the gate terminal (Figure 9). In this way, the current flow can be directly controlled by the voltage applied between the gate and the device (V_g).

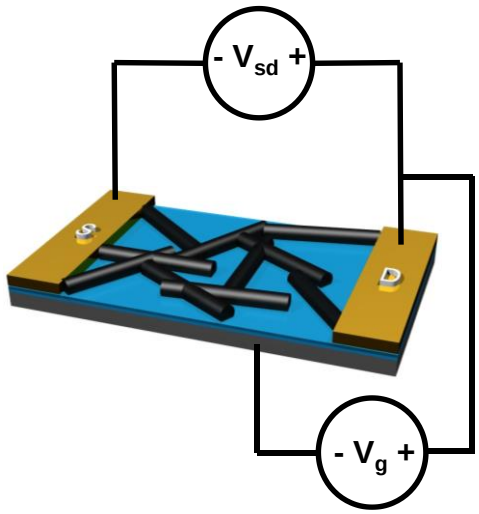

Figure 9. Cartoon depiction of a back-gated field-effect transistor. A current from source to drain is established by biasing source and drain electrodes (V_{sd}). The drain current can be modulated by a third gate terminal by injection of charge carriers through a gate biased against the device (V_g)

Field-effect transistors are generally characterized using their transfer curves. A transfer curve is a plot of the current passing from source to drain (I_{sd}) as a function of applied V_g. The transfer from "on" to "off" states can be observed and the transistor is described by the properties shown. On/off ratio is the ratio of the current represented by the on and off states and generally, a

larger ratio is advantageous. Threshold voltage is represented by the “pinch-off point” of the transistor where the gate voltage causes the device to be switched off. By observing the state of the device at negative and positive gate voltages across a transfer curve, one can determine whether the active material is p-type, n-type, or ambipolar. If a device is in the on state at negative gate voltages, it is considered a p-type semiconductor indicating that the majority carrier of the material is holes. The opposite is true for a device that turns on at positive gate voltages, which would make the majority carrier electrons. An ambipolar semiconducting material will turn on at positive and negative gate voltages, with a minimum current between both on-states commonly referred to as the charge neutrality point.

There are different ways to gate a field-effect transistor; though each method uses a third electrode to gate the device, the gate geometry and location can affect the transistor performance. Two examples are liquid gating and back gating, both of which are used in this work. In the case of liquid gating, the semiconducting material is immersed in a dielectric fluid (commonly water) and a gate electrode contacting the fluid causes capacitive charging near the material surface which electrostatically influences charge carriers in the material. Back gating involves using an insulator layer on silicon as a dielectric material for the gate electrode (Figure 9). This method also works by capacitive charging and this insulator material is usually made out of a metal oxide material (i.e. SiO_2, HfO_2, Al_2O_3). With back gating, the gating efficiency is also mainly determined by the dielectric constant of the oxide with a higher value yielding a better gate material. Hafnium oxide has shown to be a very promising gate oxide material due to its high dielectric constant.

1.4.1 SWCNT-FET

Recently, the scientific community has been working towards integration of carbon nanomaterials into consumer electronics. There are very obvious advantages to SWCNTs in transistor such as ballistic transport of electrons (little to no electron scattering),[51] high carrier density,[52] and varying band gap related to the chirality.[13] The first SWCNT-FET was demonstrated in 1998 and showed that carbon nanotube transistors were not only possible, but that they could be operated at room temperature and showed promising performance.[2] Though the properties of individual SWCNT transistors have been shown to be superior to current silicon technologies,[52] the assembly of microelectronic devices utilizing individual SWCNTs has not been practical due to the difficulty of individual SWCNT placement. Commonly, arrays of thousands of SWCNTs (random network thin films and aligned arrays) are utilized due to the ease in device fabrication on this scale. Networked arrays of nanotubes tend to show higher current output and reproducible performance.[53] Aside from issues with device assembly, control over the device characteristics which are a result of a mixture chiral species, defects, series resistance, and metallic impurity remain a current issue in SWCNT FET application. Chirality and metallic impurity can be reliably controlled through post-synthesis separations. These separations require extensive solution processing which leaves the nanotubes coated in surfactant. The surfactant coating of the nanotube wall surfaces has been shown to have a very noticeable effect on the on/off ratio of nanotube thin film transistors and it is thought that the coating interferes with tube-tube and tube-electrode connections.[54] Though there are methods to remove surfactant from SWCNT transistors,[55-56] the reality is that complete removal is very difficult due to the strength of interaction between SWCNTs and surfactant.[31] With partial removal or complete removal, transistor characteristics improve across the board likely due to

decreased contact resistance. This improvement after removal is dependent on the overall effect that the surfactant has on the device. Sodium dodecyl sulfate has been shown to alter the electronic properties greatly, likely due to its overall anionic property leading to unwanted surface charge and screening effects.[57] Transfer curve improvements are usually observed as an increase in on/off ratio and shift in threshold voltage to lower voltages.

When SWCNTs are incorporated into FET devices, a series resistance forms across the nanotube network. The largest contribution to resistance comes from the work function mismatch of SWCNTs and the electrode metal comprising the source and drain contacts of the device. When physical contact between semiconductor (SWCNT) and metal (usually gold or palladium) occurs, Fermi level pinning takes effect and band bending is observed at the interface. This contact is referred to as a Schottky barrier and results in resistance due to the energy required to overcome the energy mismatch.

Another large contribution to the series resistance of carbon nanotube transistors is barriers at tube-tube junctions along the network from source to drain. It has been found that metallic/semiconductor SWCNT contact points cause large Schottky barrier resistances.[58] These junction effects can be minimized by removing the metallic SWCNT species which is one major motivation for using semiconductor-enriched SWCNTs. The junction effects can also be lowered by aligning the network of nanotubes in a unidirectional morphology. This has been shown to dramatically improve SWCNT FET electrical properties.[59] Alignment can also be achieved by depositing nanotubes by dielectrophoretic deposition (DEP).[60] This method utilizes an alternating current (AC) waveform generator to bias source and drain electrodes at specific frequency. Depending on the peak to peak voltage and switching frequency, a favorable dielectrophoretic force can cause nanotubes to deposit between source and drain terminals

forming highly aligned networks. As nanotubes are anisotropic in shape, they align with the electric field that is generated between source and drain electrodes, forming aligned networks.

SWCNT transistors, in vacuum, exhibit ambipolar semiconductor characteristics[61] (indicating electron and hole conduction are both favorable), but in ambient conditions they are p-type semiconductors (Figure 10).[2] This is likely due to adsorbed water which is present in ambient conditions and has been shown to have very noticeable effects on SWCNT transfer curves including increased hysteresis.[62] This water present on device surfaces leads to the introduction of trap states for the charge carriers in the SWCNTs. These trap states arise from the water redox couple that lies near the fermi level of SWCNTs and these states cause the Fermi level of the system to effectively shift to lower energy, but also pulls electrons out of the nanotubes to balance the water redox reaction. Both of these effects decrease electron conduction of SWCNTs in ambient conditions.[61] This decrease in electron conduction after humidifying a device from vacuum is illustrated in Figure 10.

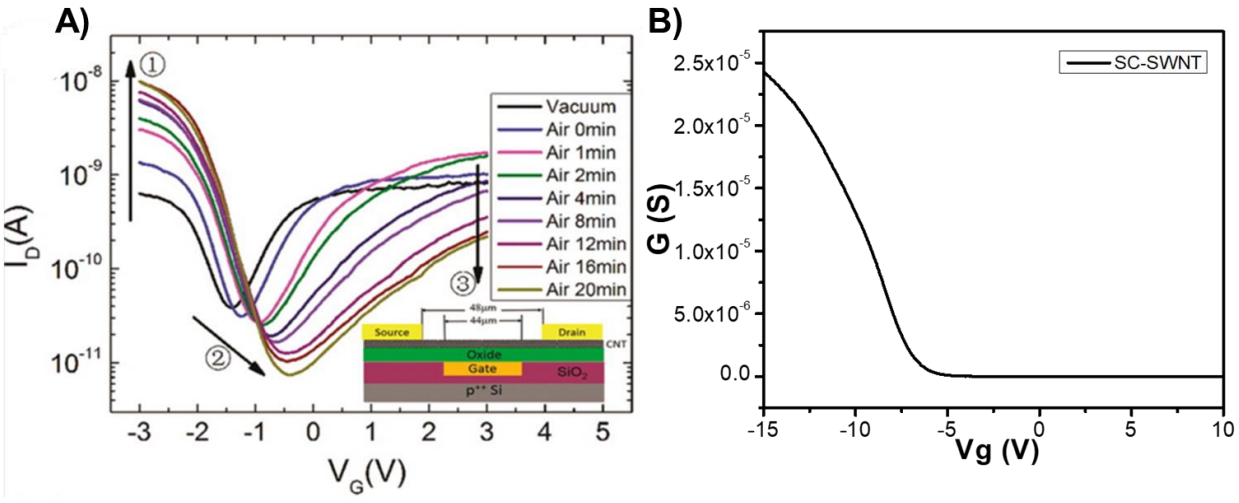

Figure 10. Ambipolar to p-type conversion upon exposure to water. A) The evolution of p-type semiconducting from ambipolar behavior of SWCNT FET after exposure to ambient conditions. Adapted with permission from [61]. Copyright 2014 American Chemical Society. B) A standard SWCNT FET curve taken in ambient conditions showing an on state at negative voltages (indicating p-type behavior)

As-synthesized batches of SWCNTs statistically contain 33% metallic nanotube content. In the SWCNT-FET field, these are commonly referred to as "metallic impurity" because metallic connections in a field-effect transistor are undesirable. Metallic SWCNTs in FET degrade device performance by contributing to series resistance when in contact with s-SWCNTs and also by increasing off current (Figure 11). Increased off current is because metallic SWCNTs are always "on" as they are invariant to gate voltage. It is advantageous to remove metallic impurity from SWCNTs for application in FET for these reasons.

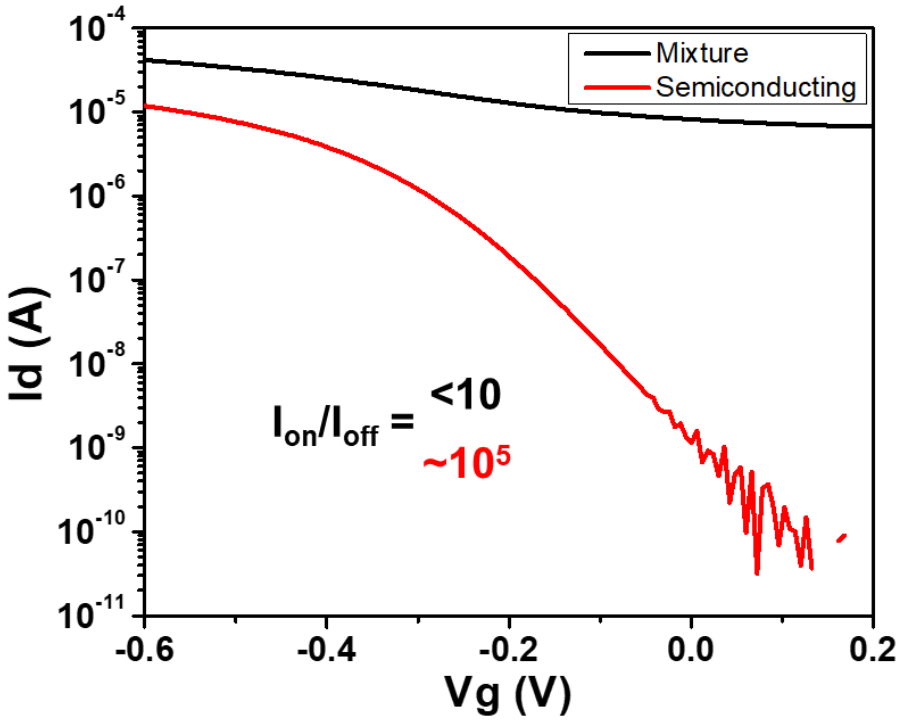

Figure 11. FET transfer curves of a mixture of semiconducting and metallic SWCNTs with a high off current (black) versus a 99.99% enriched s-SWCNT device with nearly zero off current. The on/off ratio of SWCNT transistors also dramatically increases after removal of metallic SWCNTs.

The technological roadmap for CNT-FETs requires a metallic impurity of 0.0001% or less for large scale integration into integrated circuits.[63] When these conditions are met, SWNCT FET devices can theoretically work in a low power range with low power loss when in the off state. Initial attempts to remove the metallic impurity in SWCNT networks involved selectively

burning away metallic species from a constructed SWCNT-FET by utilizing joule heating while the s-SWCNTS are in the off state. In this method, a thermo-responsive photoresist is applied to SWCNT-FETs and current is passed through the device while the semiconducting tubes are turned off. This created trenches in the photoresist specifically where metallic nanotubes are which allows for these species to be etched away in a reactive ion etch.[64] More sophisticated separation methods of separation have been described previously.

1.4.2 SWCNT-FET Sensing

SWCNTs represent an attractive transducer material for FET sensing technologies due to their impressive electrical properties (described previously), large-surface area,[65] and very sensitive response to small changes in their local environment.[66] The geometry of SWCNTs as a transducer in sensor platforms is desirable because they consist entirely of surface atoms. SWCNT-FET sensing platforms allow for a highly sensitive, label-free sensing technology.

Generally, response occurs when SWCNTs experience charge transfer either by injection of electrons or extraction of electrons from the nanotubes. FET is an ideal way to observe these changes because very minor charge transfer effects cause pronounced changes in an FET transfer curve.[67] When an electron is transferred into a SWCNT, electron-hole recombination occurs which decreases the conductance of the nanotube. This decrease is due to the fact that carbon nanotubes are p-type semiconductors in ambient conditions, and by the same logic introducing holes into the SWCNT will increase conductance.[67] This decrease in conduction presents itself as a horizontal translational shift of the FET curve. Heller *et al.* explored the effects of different sensing mechanisms on the FET curve of liquid gated devices based on computation.[68]

Interestingly, the effects of different nanotube chiralities on detection of analytes have not been thoroughly explored. This is not to say that single chiral SWCNT FETs have not been constructed. There have been reports of assembly of single-chiral SWCNT FETs, with the first published single-chiral FET published in 2009.[69] Hydrogen sensing has been explored with comparing (9,7), (7,5), and (6,5) SWCNTs and each species showed very different sensitivity to detecting the hydrogen gas.[5] It is expected that the chiral angle, band gap, and diameter will play a significant role in analyte binding and interaction. Having a fundamental understanding of these interactions could lead to further optimization of state of the art SWCNT FET sensing technologies.

1.4.3 SWCNT-FET Memory Devices

Memory devices are very important to our everyday lives as they are responsible for storing our data and memory plays an integral role in active computing. In our current digital age, memory plays a vital role in the archival and retrieval of information. As we generate more data through social media, digital news outlets, high definition video and photography as well as many other sources, the need for massive data centers and cloud computing has become commonplace. As humanity continues to require more storage, there is a focus on higher capacity memory devices through shrinking the physical size of memory devices.

In computers, memory refers to any and all devices that store any form of information. This can refer to hardware that stores memory for very short periods of time that is quickly passed on or constantly re-written, for example random access memory (RAM). This type of memory quickly disappears when not monitored and maintained and thus requires constant power. Due to these properties, memory such as RAM is referred to as volatile memory. Volatile

memory plays a critical role in computing as it is used to very quickly store data and be read by other components. Data and instructions can be temporarily stored in RAM before either being sent to the central processing unit (CPU) to be interpreted as instructions or be saved elsewhere in a more permanent location. The other type of memory, called non-volatile memory, is used in computers to permanently store information. Non-volatile information can be stored and retained even after power is removed and thus does not need constant monitoring to retain the information stored within. Examples of non-volatile memory are hard drives, optical discs (such as a CD or DVD), and even paper tape. Paper tape, one of the most primitive forms of nonvolatile memory, was used in the 1950s by computers to input program instructions and store data. Paper tape is simply a strip of paper with holes punched in it and the series of punches and their location could be interpreted by the computer to execute commands. The most recent advancement in nonvolatile memory is in the form of solid state hard drives. These work by storing data as flash memory which works by trapping charge in individual memory cells. An individual memory cell serves to store an individual bit which is usually stored as a 1 or a 0. Stored charge can be read as a high current (1) and empty cells can be read as low current (or a 0). Although data can be stored without constant powering in solid state hard drives, once data is read, this discharges the memory cells read and they have to be rewritten to retain the information. Due to this constant re-writing of accessed information, flash memory devices tend to have shorter lifetimes than traditional mechanical storage solutions such as the hard disk drive.

Some important parameters when characterizing memory cell devices are bit retention time, cycle stability (endurance), and bit separation. Bit retention time is the time that a memory cell can retain information while not being constantly powered. This parameter is what determines whether a device is considered non-volatile or volatile memory, though there is no

clearly defined cut off time between both types of memory. This leaves an area in between volatile and non-volatile memory that can be considered a slow leaking non-volatile memory or a long lasting volatile memory. Bit retention is tested by writing a bit and reading over time until both bit states collapse upon each other (Figure 12A). Bit endurance is tested by cycling a memory cell device through multiple memory cycles to test cycle stability of the device. A standard memory cycle is writing a 0 (commonly called erase), reading the bit, writing a 1 (commonly called program or write), and reading the bit (Figure 12B). This sequence is commonly abbreviated as an E/R/P/R cycle. For a SWCNT-FET based memory device, all 4 operations are controlled by changing the gate voltage applied to the material. Erase and program voltages are a nonzero voltage of opposite sign to each other and reading is generally done at 0 V_g.

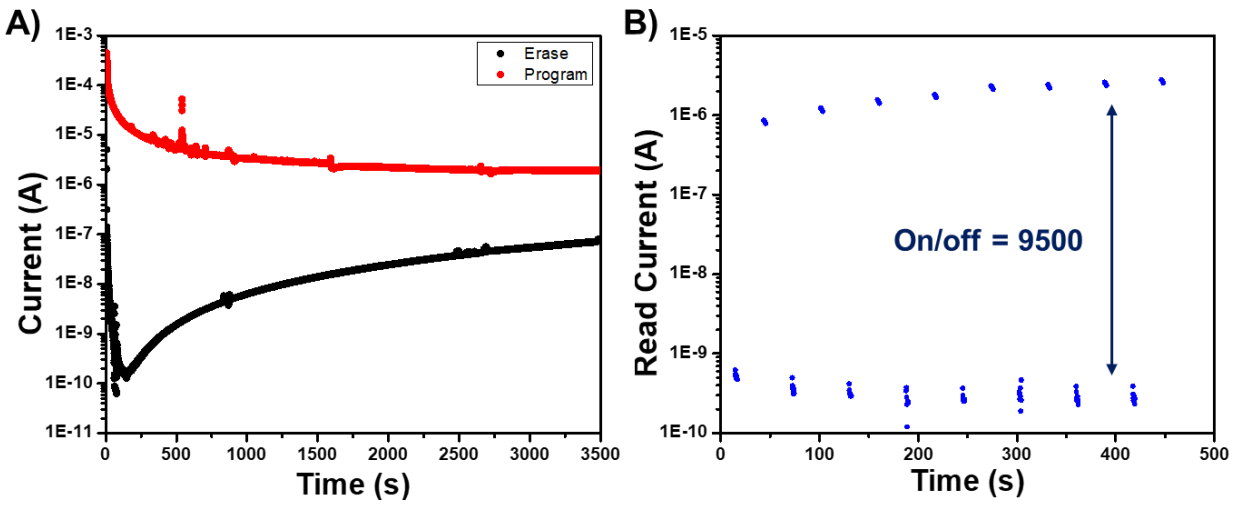

Figure 12. Memory parameter tests. A) Bit retention test of a SWCNT-FET based memory cell. The separation between both bit states (0 and 1) decrease over the course of an hour, but are still separated by more than an order of magnitude. B) Bit separation measured from a cycle endurance test over 8 cycles. A current separation of ~10^4 was observed.

Carbon nanotubes have been proposed as a potential alternative material for solid state storage devices and have shown very impressive retention, endurance, and bit separation.

SWCNT-FET based memory cells face challenges with large scale integration, reliability, and speed. Many improvements to these materials must be made to compete with silicon-based flash memory which is widely used due to its reliability, low cost, and fast performance.

1.5 ALTERNATING CURRENT MEAUREMENTS

Chemical sensor research utilizing direct current (DC) sourcing and measurement with SWCNT-FET devices have been explored for more than a decade. Though there have been many developments in this field since its inception, there are some clear drawbacks to DC sensors. Alternating current-based measurement schemes for SWCNT-based chemical sensors to counteract many of the issues with DC sensors. The AC heterodyne method was applied by Girish S. Kulkarni in the Zhong group at the University of Michigan.[70] The motivation for developing an alternative to DC measurements with SWCNT-based vapor sensors was due to the fact that in the vapor phase, molecules are charge neutral. As charge transfer interactions require strong binding to the sensor surface,[71] measuring neutral molecules in the vapor phase with pristine carbon nanomaterials is not a favorable process.[72] SWCNT-based DC gas sensors generally have slow response and recovery times and this behavior is a direct result of the strong binding necessary for vapor sensing to occur. Kulkarni *et al.* have applied this AC heterodyne method to protein sensing in high ionic strength solutions[73-74] and chemical vapor sensing with graphene.[75-76]

1.5.1 Theory of AC Heterodyne

The source signal for AC heterodyne is an amplitude modulated sine wave voltage source. The concept of amplitude modulation was first introduced by Reginald Fessenden which created the foundation for AM radio around 1900. Later on, in 1918, the superheterodyne receiver was developed by Edwin Armstrong. The superheterodyne receiver, though mainly utilized for radio communications, is the main concept utilized in the AC heterodyne sensor described here.

When two frequencies are mixed together, the product is the sum and difference of the two initial frequencies. Frequency mixing results in an amplitude modulated wave with character from both initial frequencies (Figure 13A). Using this method, one can create a system where all of the sensing interactions occur at a high frequency, but detection is carried out at the low frequency, the difference between both initial frequencies ($f_1 - f_2$).[70]

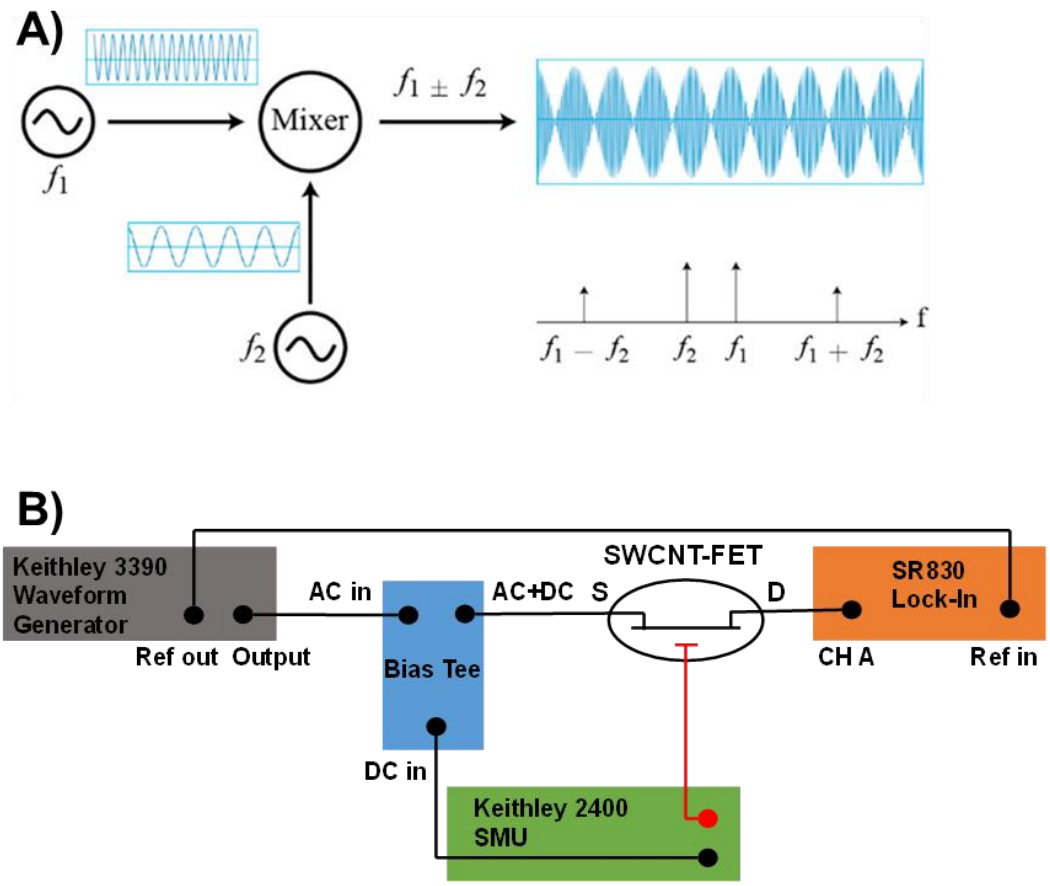

Figure 13. Principle of the AC heterodyne sensor (Reprinted with permission from [70] Copyright 2016 American Chemical Society). A) Frequency mixing of two input frequencies (f_1 and f_2) to give an amplitude modulated wave. B) AC heterodyne setup for the detection of molecular dipoles using a carbon nanomaterial FET device.

In order to utilize the AC heterodyne sensing method, Kulkarni *et al.* set up a three terminal FET device with an amplitude modulated AC voltage bias between source and drain (Figure 13B). According to Ohm's law, current is equal to the product of conductance and voltage. By incorporating AC voltages into this expression, one can get a general expression for all current signals related to conductance and voltage:

$$I = (G + G_\omega) * (V + V_\omega) = (G * V) + (G_\omega * V) + (G * V_\omega) + (G_\omega * V_\omega) \quad (4)$$

Where I is current in amps, G is conductance in Siemens and V is voltage in volts. All terms with a ω subscript represent AC components. The first three terms on the right side of this expression represent traditional DC sensing, impedance/capacitance sensing and noise sensing.[75] This setup, when coupled with a lock-in amplifier locked in to the modulation amplitude of the wave (the lower frequency of the two input frequencies) detects the mixing current from the FET device. All DC effects are ignored when looking solely at the mixing current (I_{mix}) resulting in a sensor signal proportional to the dipole moment of molecules near the device surface as opposed to charge transfer.[70]

2.0 SWCNT CHIRALITY SEPARATION AND SENSING

2.1 COLUMN CHROMATOGRAPHY OF SWCNTS

The focus of this project was based on SWCNT-FET sensing utilizing single-chiral semiconducting SWCNTs. In order to begin these studies, published procedures were utilized to obtain highly enriched single-chiral SWCNT samples as these materials are not commercially available. Many different methods were explored including aqueous two-phase separations as well as many modifications to published column chromatography separations. This work is primarily based off of Liu *et al.*[17] with modifications introduced from optimized procedures utilized by Tvrdy *et al.*[40] This work was successful in producing four different chirality-enriched samples in appreciable yield.

2.1.1 Experimental

2.1.1.1 HiPCO SWCNT Solution Preparation

15 mg of purified HiPCO SWCNTs (Unidym) were added to a 2% by weight SDS solution in water (15 mL) to make a 1 mg/mL solution. The nanotube solution was then briefly bath sonicated (5 min) to roughly disperse SWCNTs in solution prior to tip sonication. This solution was then further sonicated using a tip probe sonicator (FB505 Sonic Dismembrator, ½" titanium probe tip) for a total of 16 hours of "on" time while being cooled by an ice bath. This

was performed at a 45 sec. on/15 sec. off duty cycle in 1 hour intervals. In between 1 hour runs, the ice bath was replenished to keep the temperature of the solution fairly constant throughout the full run. This solution was then placed in an ultracentrifuge (Beckman TXI) at 21,000 RPM (190,000 g) for 4 hours to separate bundled SWCNTs. The top 80% of the supernatant was recovered for column chromatography separation as a stock solution of monodisperse SWCNTs.

2.1.1.2 Column Chromatography of SWCNTs

Column chromatography was performed in 20 iterative 10 mL columns as the gel volume necessary for separations was small. Each column was constructed by closing the bottom with a small cotton plug and filling with a slurry (water/ethanol mixture) of Sephacryl HR200 gel medium to a volume of 1.4 mL under ambient pressure. Before use, each column was thoroughly washed with 2% SDS solution (2.5 column volumes). For the first column, 10 mL of stock solution was applied and the first fraction was collected (labeled “next”). 4 mL of 2% SDS solution was then added to the column and a second fraction was collected (labeled “waste”). Waste will mostly contain metallic nanotubes. Finally, 4 mL of 5% SDS solution was applied to the column to desorb loosely bound nanotubes and “fraction 1” was collected. The “stock” for the next column was then applied to a second column and the procedure is repeated until 20 iterative column separations are performed.

2.1.1.3 Analysis of SWCNT Chirality Content

After observation of absorption spectra, it was determined that metallic nanotube content in the samples was small. An assumption that metallic SWCNTs were completely removed was used during analysis based on this observation. This analysis was performed by careful deconvolution of absorption data obtained by UV-vis-NIR measurements using known peak

wavelengths for different chiralities as well as a knowledge of which chiralities are present in a HiPCO batch sample. Deconvolutions were performed in OriginPro 8.5 utilizing the Peak Fitting feature by assigning peak wavelengths observed in the spectra and lorentzian peak profiles. From these deconvolutions, percent abundance of chirality content was calculated based on peak area divided by total peak area analyzed.

2.1.2 Results of Chromatographic Separations

Column chromatography experiments yielded solutions with reasonably high percentages of 4 different chiralities as determined by absorption spectrum deconvolutions (Figure 14A). As expected, chirality-enriched solutions exhibit interesting optical properties based on the band gap of SWCNTs in solution (Figure 14). These experiments yielded (8,4), (6,5), (7,5), and (7,3) solutions of appreciable enrichment. Due to the harsh solution preparation conditions requiring long tip probe sonication, it was expected that the stock solution used for separations may be fairly defective. Raman spectroscopy was used to characterize the presence of defect states on the stock solution of SWCNTs prior to separation and found very little defect density as evidenced by the low D/G ratio (Figure 14C).

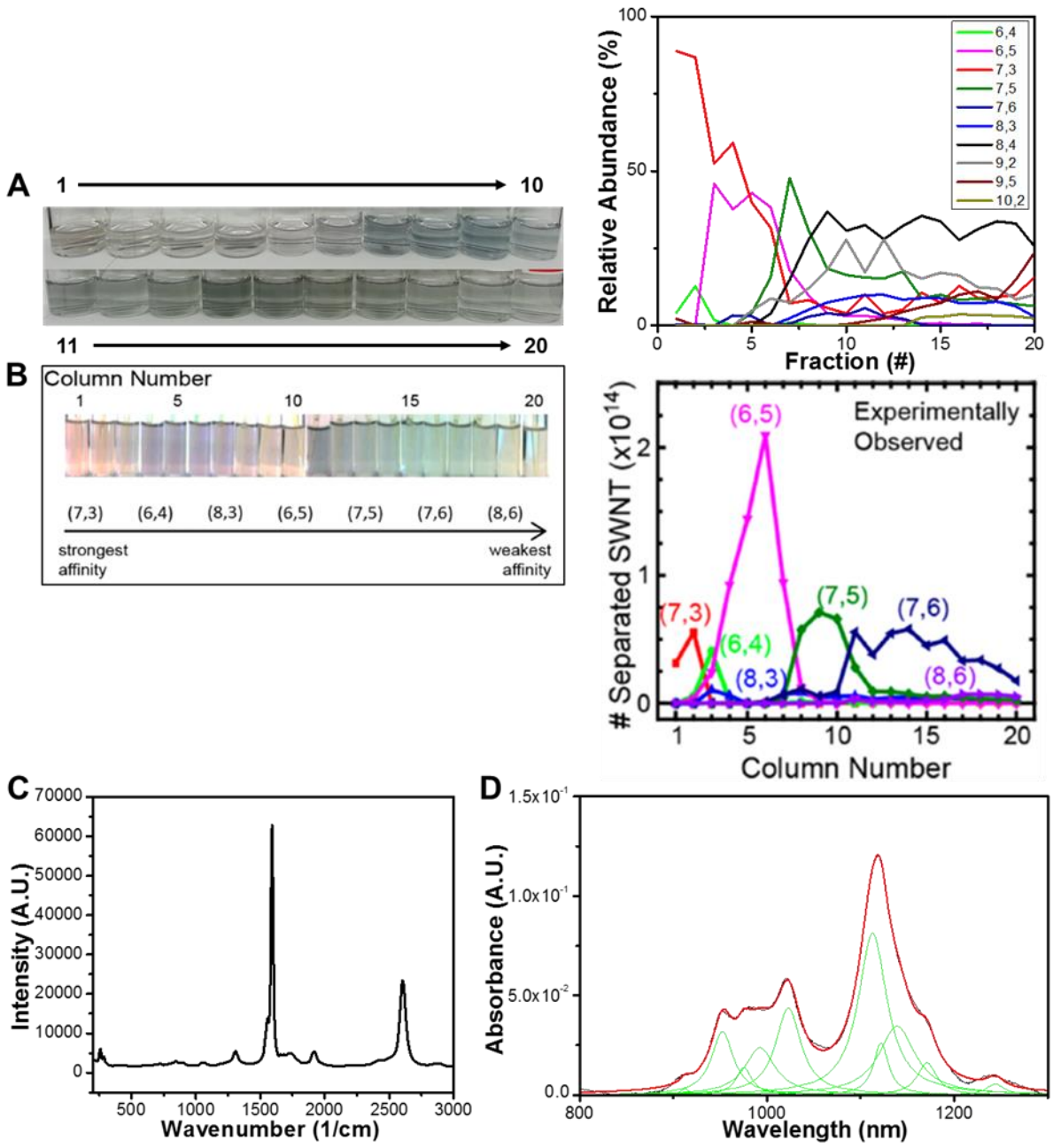

Figure 14. Chirality separation summary. A) left: image of SWCNT solutions from fraction 1 to 20; right: elution profile expressed in relative abundance of each chirality. B) left: Image of SWCNT solutions from fraction 1 to 20; right: elution profile expressed as # of nanotubes of each chirality. Reprinted with permission from ref [40]. Copyright 2013 American Chemical Society. C) Raman spectrum of HiPCO SWCNT solution prior to separation (D/G = 0.131 ± 0.018), indicating very little defects. D) Example of deconvolution of absorption data to get nanotube chirality distributions.

It is clear that the obtained results do not agree very well with the expected separation efficiencies obtained in the literature (Figure 14A, B). This can be due to a few factors: 1) Sonication may need to be run constantly and not on a pulse (this would require a cooling apparatus). This is not specified in the literature. The evidence for this is the fact that only the most abundant SWCNT species (from a batch sample of HiPCO) were successfully enriched. 2) The column setup may not be optimal or fit specs of the previous research. Gel volume from column to column varied by about 0.3 mL on average from the desired 1.4 mL. 3) Column overpressure was not controlled in these experiments. Some procedures call for a 1 mL/min flow rate controlled by a syringe pump while others do not. This could result in differences in binding kinetics over time as solution filters through the column.

2.2 SENSING OF MONO-SUBSTITUTED BENZENES WITH SINGLE-CHIRALITY-ENRICHED SWCNT-FET

Single-chiral SWCNT sensors are on the forefront of fundamental research in chemical sensing with carbon nanotube FET. It is a largely unexplored field due to the difficulty of device assembly with surfactant-coated SWCNTs and the limited commercial availability of single chirality nanotubes. This project was largely motivated by work previously published by Star *et al.* in 2003.[77] In this work, it was shown that nanotube FET response can linearly correlate with the Hammett constant of mono-substituted benzene species. These species were chosen because they are structurally similar and should bind similarly, but they have different substituents which lead to different properties. The SWCNTs used in this study were CVD-grown nanotubes and

consist of a mixture of many chiralities as well as metallic nanotubes. The response observed in this work is a result of the summation of the response of all chiralities transducing the signal.

To further this work, we sought to show how individual chirality enriched nanotubes would respond to monosubstituted benzenes. It is not unreasonable to think that the differences in chiral angle and diameter of SWCNTs would play a role in binding, as it has been shown with hydrogen sensing.[5] It is expected that the electronic properties, chiral angle, and diameter play a role in analyte binding and sensing. In a proof of concept experiment, chirality enriched SWCNTs collected from the previous separation experiments were used to fabricate FET devices. The devices were exposed to solutions of mono-substituted benzenes and response of the devices were recorded and plotted against the Hammett constants of the species tested.

2.2.1 Experimental

2.2.1.1 Photolithography Procedure

Prime grade silicon wafers (1000 nm wet thermal oxide, SSP, 4" diameter, Silicon Quest) were purchased from Silicon Quest International through the Nanofab at Carnegie Mellon University. The wafer was cleaned utilizing a solvent bath and sonication method to remove residues. The wafer was immersed in a bath of acetone and sonicated for 30 seconds. This was performed twice more with acetone. The wafer was then cleaned in isopropyl alcohol, methanol, and DI water baths following the same procedure. The wafer was hosed off with DI water and dried with nitrogen. To promote adhesion of the primer, the wafer was further dried on a hotplate (150°C, 1 minute) to drive off remaining water. The wafer was primed with a spin coating procedure (Laurell Technologies WS-400B-6NPP-LITE; Step 1: 10 s, 500 RPM, Acc 3; Step 2: 30 s, 5000 RPM, Acc 7) using an HMDS-based primer (MCC 80/20). This was followed by

photoresist coating (Shipley 1805) using the same spin coater parameters used for primer. The wafers were visually inspected for defects in the photoresist coating (comets, streaks, bumps). The wafer was then soft baked (115°C, 30 s) to harden the photoresist and allowed to cool on a clean pad, covered for 5 minutes at room temperature. The wafer was exposed to the desired pattern (Quintel Q4000 MA, 8.2 s exposure, pressure contact mode) and developed to remove exposed photoresist (351 Developer, 1:5 v/v with water, 45 s). The wafer was washed with DI water and dried with nitrogen. It was then briefly cleaned with oxygen plasma (Trion Technology Phantom III LT, 60 s, 100W forward, 200 mTorr operating pressure, 10 sccm oxygen) and hard baked to further solidify the photoresist (115°C, 3 min). Lastly, the wafer was coated with titanium and gold in an e-beam evaporator (Thermionics Laboratory VE180, 15 nm, 50 nm). Excess metal was lifted off in acetone and diced at the Nanofab at Carnegie Mellon University.

2.2.1.2 FET Measurements

FET measurements were performed with 2 Keithley 2400 Sourcemeters configured for 3 terminal operation (source, drain, gate) operated through LabView. Liquid gating was performed from $+0.6V_g$ - $-0.6V_g$ (Ag/AgCl gate electrode) to avoid water oxidation/reduction and plotted as drain current as a function of gate voltage.

2.2.1.3 SWCNT FET Device Fabrication

SWCNTs were drop cast onto pre-fabricated 4-device chips. 3 microliters of SWCNT solution were dropped onto a chip and dried on a hotplate (~120°C) to remove solvent and immobilize SWCNTs on the surface of the device.

2.2.2 Sensing Results

For these experiments chirality enriched (7,6) SWCNTs from the column chromatography separations were used to sense nitrobenzene, aniline, and phenol. Sensing with chirality enriched SWCNT-FET and the relationship between the response to monosubstituted benzenes and their Hammett constants have not been explored. The metric that was used to quantify the sensing response to different benzenes is the threshold voltage change of the device. This parameter was chosen as it was previously shown that charge transfer is the dominant sensing mechanism for this system. This results in a translational shift of the FET curve which can be observed by a change in threshold voltage (Figure 15).

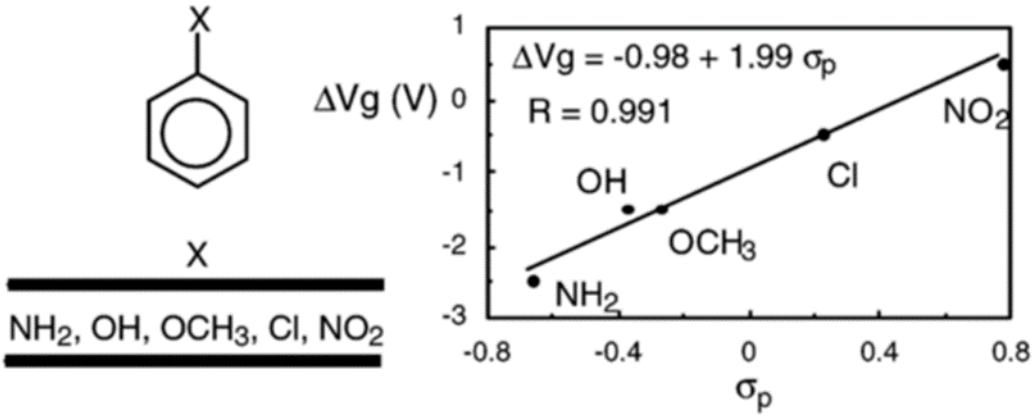

Figure 15. Results from sensing experiments comparing the translational shift of the FET curve (ΔV_g) to the Hammett constant of a selection of 0.1 M solutions of mono-substituted benzenes in cyclohexane. Reprinted with permission from reference [77]. Copyright 2003 American Chemical Society.

The previously performed experiments utilized back-gated FET as they were taking measurements in cyclohexane, which lacks a dipole. This lack of dipole and charge makes cyclohexane a poor solvent for liquid gating due to a low dielectric constant. The experiments that were performed utilized liquid gated FET for device measurements due to higher gating efficiency achieved in a liquid gated FET. The liquid medium chosen for gating was water due to

its high dielectric constant. Gate sweeps were kept within the electrochemical window of water (0.6 V to -0.6 V) to avoid water oxidation and reduction. Solutions of nitrobenzene, aniline, and phenol in water (4 mM) were analyzed by a device fabricated with (7,5) SWCNTs. Between measurements, devices were rinsed with excess water to completely remove residual analyte from previous tests. It is clear that a different response is observed when the device is exposed to these selected analytes, as expected (Figure 16A). In these experiments, threshold voltage is measured by the linear extrapolation method.[78] Accounting for hysteresis by taking the FET scan in the opposite direction (- to + gate voltage), one can take the average of threshold voltage values measured in each sweep direction. This gives a much more accurate threshold voltage value accounting for hysteresis and charging effects and shows a fairly linear relationship with Hammett constant values (Figure 16B).

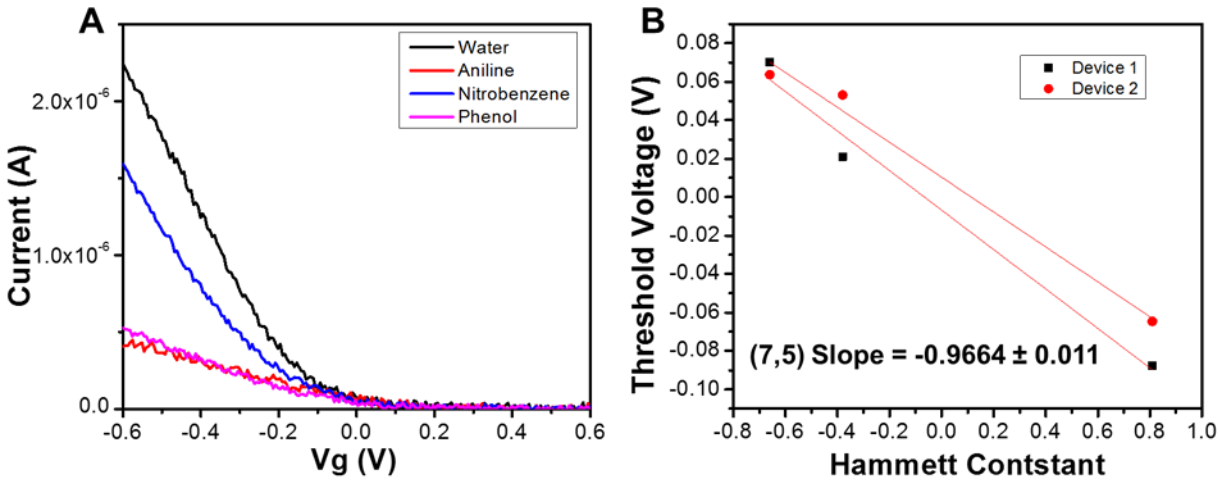

Figure 16. (7,5) SWCNT sensing data**.** a) FET curves of (7,5) SWCNT device before (water) and after exposure to analytes. Clearly, a change occurs upon exposure to each species. b) Extrapolated threshold voltages from FET data plotted against the Hammett constants of each species measured.

In conclusion, it was found that chirality enriched (7,5) SWCNT-FET sensors respond to monosubstitued benzenes linearly with respect to their Hammett constants. This linear relationship is similar to what was observed previously for mixtures of SWCNTs. As the

Hammett parameter is an empirical value which categorizes the electron donating or withdrawing ability of substituents, the linear relationship observed in these experiments further suggests that the sensing mechanism here is dominated by charge transfer interactions. These charge transfer interactions are observed through the charged surfactant coating on the SWCNTs. As part of the proposed mechanism of column separations explored previously in the introduction, SDS adopts different wrapping conformations dependent on the chirality of the SWCNT. This difference in wrapping morphology would likely cause different sensing response to monosubstituted benzenes depending on the density of charged surfactant coating the SWCNT surface.

3.0 POLYMER HYDRATE CRYSTALLIZATION IMPROVES CARBON NANOTUBE MEMORY

This submitted manuscript is a collaboration with the Keith and Velankar groups in the Swanson School of Engineering at the University of Pittsburgh, the Department of Geosciences at SUNY, and DuPont Central Research and Development. This work is focused on the interesting phase behavior of poly(oxacyclobutane) (POCB) in mixtures of water, forming a semicrystalline material. The proton conduction of the material was utilized to improve the memory properties of SWCNT-FET based memory devices utilizing s-SWCNTs.

List of Authors: Michael T. Chido, Peter Koronaios, Karthikeyan Saravanan, Alexander P. Adams, Steven J. Geib, Qiang Zhu, Hari B. Sunkara, Sachin S. Velankar, Robert M. Enick, John A. Keith, Alexander Star

3.1 INTRODUCTION

Due to their superior electronic properties,[51, 79] nanometer-sized dimensions,[80] and mechanical strength,[81] single-walled carbon nanotubes (SWCNTs) have been applied in a wide array of applications spanning many fields of chemistry and engineering. In particular, SWCNTs have shown to be a promising material when used in field-effect transistor (FET) devices for chemical[67] and biological[82] sensing, high-performance electronics,[83-84] and memory storage

materials.[85-88] SWCNTs are synthesized as a mixture of semiconducting and metallic nanotubes, but high performance FET devices require the removal of metallic nanotube species.[89-90] Removal of metallic species allows for low power operation by decreasing the current flowing through devices in the off state to nearly zero.[91] Decreasing off current also allows for dramatic improvement of on/off current, defined as the maximum current in the on state divided by the off current. A high on/off ratio allows for more separated on and off states which is a necessary requirement for high performance transistor-based memory. High purity semiconducting SWCNT (s-SWCNT) inks have become increasingly available commercially and this availability allows for cutting edge research with development of highly pure s-SWCNT-FET devices.

It is known that the transport properties of SWCNT-FETs are heavily influenced by the environment when operated in ambient conditions.[61-62] When SWCNT-FETs are measured in ambient conditions they act as p-type semiconductors,[92] thought to be a result of their interaction with ambient oxygen and water leading to direct doping effects from oxygen molecules and the creation of low lying trap states due to the water redox couple.[61] For traditional back-gated SWCNT-FETs, the presence of water on the gate oxide surface and SWCNT network surface is undesirable as it introduces large hysteresis effects during operation.[62] For memory storage applications, hysteresis is a necessary property of a material as it allows for storage of information. In transistors with hysteresis, the threshold voltage is dependent on the measurement conditions such as the direction in which gate voltage is swept. This difference in threshold voltage is also known as the memory window and in memory applications, a large memory window is desirable. Memory can be generally classified as non-volatile (NVM) or volatile memory (VM). NVM materials store information and retain this stored data even after power cycling, whereas VM stores information but loses this information when not powered.

SWCNT-FET-based memory devices have been demonstrated in the literature as promising NVM and VM materials.[85-88, 93-97] Generally, these devices work by trapping charge, either in the gate oxide[93] or in a passivation coating applied to the SWCNT network.[87, 96] NVM devices have slow charge recombination while VM devices quickly recombine charge. In this work, we take advantage of the capacitance of a polymer/water co-crystalline coating to induce hysteresis in s-SWCNT-FET devices. The capacitance electrostatically gates the s-SWCNTS and produces a large difference in current between the two states in the hysteresis loop at zero gate voltage. The states are separated by nearly 4 orders of magnitude in current, making this simple material suitable for memory storage.

We utilize poly(oxacyclobutane) (POCB), also known as poly trimethylene oxide, poly trimethylene ether glycol, poly(1,3-propane diol), poly(oxetane), or poly propylene glycol with a linear monomeric repeat unit) with a molecular weight of 650, which spontaneously forms polymer hydrate crystals with water at room temperature. The crystals melt at 38°C, far above the melting temperature of either the polymer (14°C) or water. Unlike prior reports of POCB hydrates using high molecular weights that are solid at room temperature,[98] to our knowledge, this is one of the only examples of two substances that are liquid at room temperature and spontaneously freeze upon mixing at room temperature.

3.2 RESULTS AND DISCUSSION

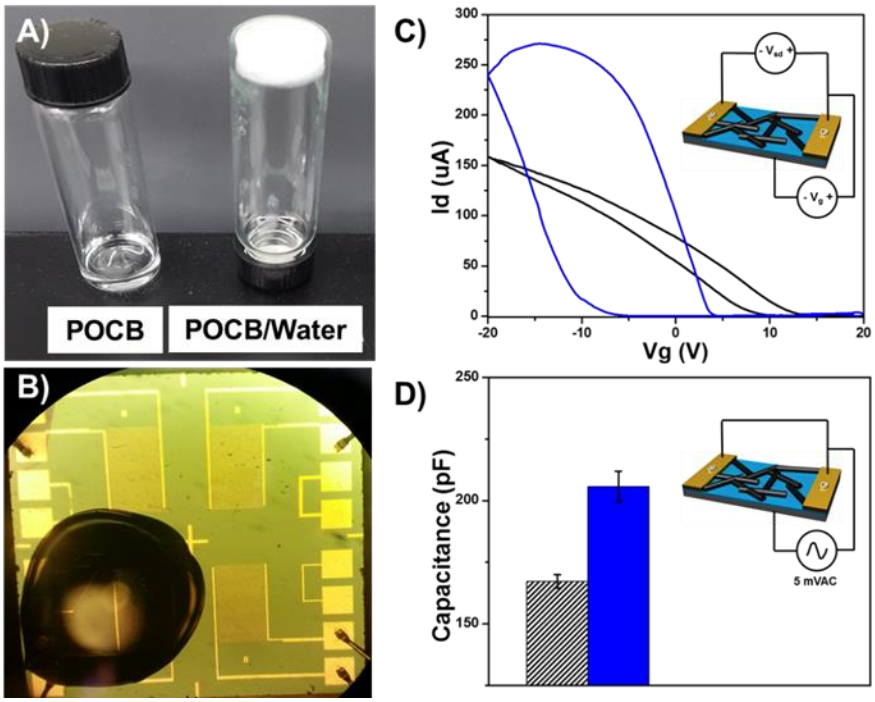

Figure 17. A) POCB/water mixture completely crystallized. B) Optical microscope image of a device coated with POCB. C) s-SWCNT device measured in ambient (black) and after coating with POCB (blue). A large improvement in device performance was observed. D) Capacitance of the nanotube network (black) and after coating with POCB showing an increase in capacitance of 38pF.

At room temperature, POCB completely co-crystallizes with water at a water:monomer ratio of 1:1 (1:3 weight ratio) to form a white solid (Figure 17A). FET devices used in this work were fabricated by photolithography and s-SWCNT ink[99] (Isosol-S100, Raymor Industries Inc.) was deposited between source and drain electrodes using dielectrophoresis (10 V_{pp}, 100 kHz, 1 min). The devices were operated in a bottom contact, bottom gate configuration. When POCB was deposited on an s-SWCNT-FET device (Figure 17B), excess polymer spontaneously crystallized with the trace water present on the surface of the silicon oxide and the carbon nanotube network. This process caused a dramatic change in FET transfer characteristics of the

device (Figure 17C). An increase in hysteresis was observed after coating and incubation for 1 hour. This incubation allows for stabilization of the device as the FET curve immediately after coating changes during the first hour, likely due to equilibration with ambient humidity. This magnitude of hysteresis in the POCB-coated FET devices can be described by a parameter called the memory window which was observed to be 15 V (Figure 17C). Notably, the POCB-coated device displayed ambipolar transport characteristics as well, indicating that the trap effect of water presence on the nanotube surface is removed. It has been shown that the p-type conduction in SWCNT-FETs operated in ambient is mostly due to the oxygen-water redox couple whose energy level lies near the conduction band of the CNTs.[61] This available trap state causes poor gate control over electron conduction in SWCNT-FETs.[61] We hypothesized that the increase in hysteresis of POCB-coated devices was caused by capacitive charging effects of POCB crystals electrostatically gating the s-SWCNTs. This capacitive charging was investigated by applying AC impedance measurements to quantify the change in capacitance after POCB coating. By applying a 5 mV AC wave through the gate oxide and detecting the –90° out of phase impedance with a lock-in amplifier, we quantified the total capacitance of the s-SWCNT-FET device before and after POCB coating and found an increase in overall capacitance (Figure 17D). The capacitance of the s-SWCNT-FET device of 167 pF represents the capacitive contribution of the 300 nm SiO_2 insulating gate oxide and the capacitance of the surfactant-coated s-SWCNT network. After POCB coating on the same device, the capacitance increased by 38 pF. This contribution is from the POCB/water crystal material on the oxide surface that acts as a parallel capacitive pathway to the s-SWCNTs, represented as a higher overall capacitance value.

The current separation at a zero-gate voltage in the FET hysteresis loop was on the order of ~10^4 amps. Due to this and the large memory window of 15 V, we applied this material for

memory storage. We utilized the gate voltage parameters used in FET to design a transistor-based capacitive memory cell. Ideally, memory cells are read at zero gate potential to avoid charging effects. These charging effects at non-zero read voltages can lead to significant drift and unwanted collapse of the stored states. Based on our FET characterization of POCB-coated s-SWCNT-FET devices, we utilized a 5 second +20 V gate pulse to erase, which puts the device in the low current state at zero gate voltage. A bit is "programmed" by a 5 second –20 V gate pulse. All bits were read 12 seconds after the program and erase pulses while applying zero gate voltage (Figure 18A, inset).

First, an s-SWCNT device was tested in ambient conditions without the POCB coating (Figure 18A). Due to the hysteresis present in s-SWCNT-FET devices measured in ambient conditions, two current states were observed in the memory test. The separation of the bits, described by an on/off current ratio of "1" divided by "0," was less than 10 which is far below the ideal bit separation of high performance memory devices (at least 10^3 to 10^4). After a POCB coating was applied to the same device, a dramatic improvement in bit separation was observed (Figure 18B). Interestingly, the 1 and 0 states of the bare s-SWCNT-FET device were reversed when compared to POCB coated devices.

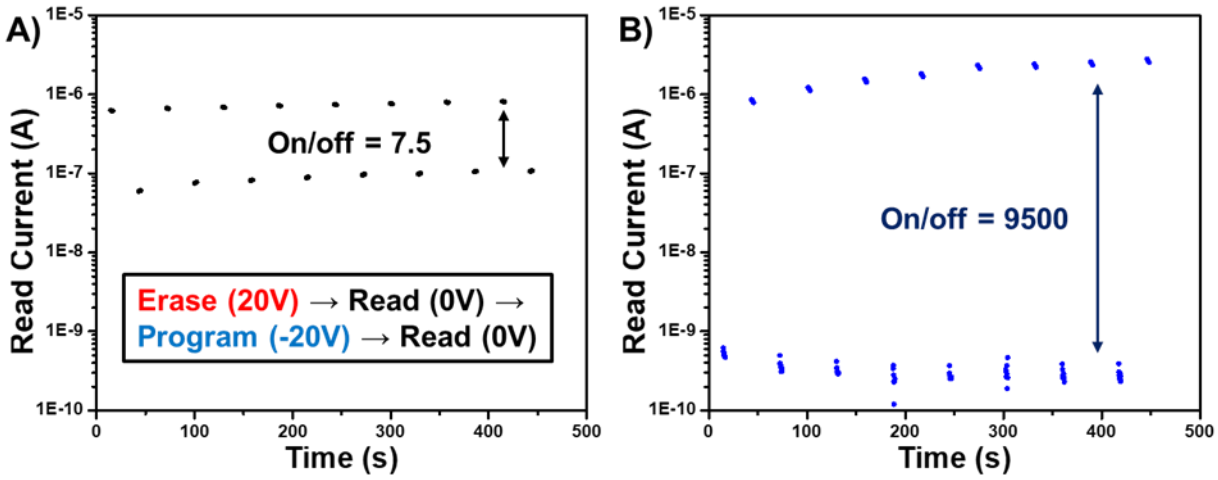

Figure 18. Application of POCB-coated s-SWCNT-FET devices for memory storage. A) s-SWCNT-FET device showing bit separation of ~10 with voltages applied for E/R/P/R cycles (inset). B) POCB-coated s-SWCNT-FET device showing bit retention and separation of ~10^4.

Bit storage was stable over the 8 cycles tested and demonstrated low and stable off currents of ~300 pA (at the limit of detection of our probing station setup). Longer cycle tests were performed on the POCB devices and they were found to endure at least 100 cycles even after 3 months of storage. Bit retention of both 1 and 0 states was tested to observe the transient behavior of the two states. After 1 hour, the current states were still separated by more than an order of magnitude. This long-term stability suggests the potential application of this material in non-volatile memory applications.

We found that the existence of polymer crystals is vital for high hysteresis to be observed in s-SWCNT devices. Removing water by heating at temperatures in excess of 100°C destroys the POCB-hydrate crystals as water is critical for crystal formation. A POCB-coated s-SWCNT device FET transfer curve was taken and the device was heated at 120°C for 1 hour in an oven, allowed to cool to room temperature and another FET transfer curve was taken. We observed that the hysteresis of the device after heating was dramatically decreased and device properties deteriorated (Figure 19A).

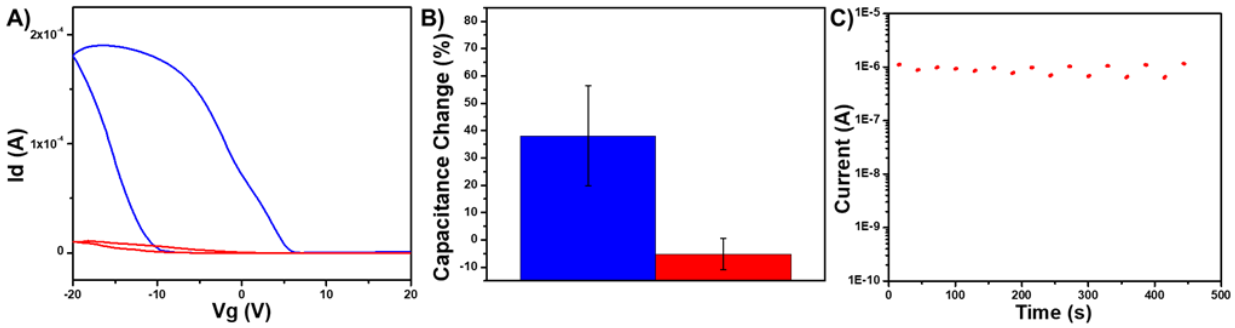

Figure 19. Characterization of POCB-coated devices before (blue) and after (red) removal of water by heating. A) FET curves indicate that the large hysteresis observed in POCB-coated devices is dependent on POCB-hydrate crystal formation. B) Change of capacitance compared with a s-SWCNT-FET device before POCB coating showed an increase in capacitance after coating with POCB and the loss of capacitance after heating. C) Memory test of a heated POCB-coated device showing bit separation failure.

This effect was also observed when looking at the capacitance of the devices using impedance measurements. When comparing with the s-SWCNT-FET devices before coating, POCB coating causes an increase in capacitance of the material. After heating, this increase in capacitance drops back to pre-POCB coating levels (Figure 19B). We also observed that the memory effect in heated devices is lost indicating that the presence of the hydrate crystals is critical (Figure 19C). The large increase in bit separation and hysteresis with the POCB coated devices is due to the capacitive charging of the POCB hydrate crystals. We also measured memory cycles of a structurally similar polymer of comparable molecular weight, poly(tetrahydrofuran) 650 (p(THF)), which does not form polymer hydrates. Compared with POCB devices, the p(THF) device showed two orders of magnitude decrease of current separation, indicating the importance of the water co-crystals for SWCNT memory. We also tested the POCB-coated device with 5 V erase (+5 V) and program (-5 V) steps and found that the on/off ratio decreases by an order of magnitude, though the bit separation decreases to 10 after 20 minutes. After a program or erase voltage pulse is applied, the POCB charges up causing

a local electrostatic gating environment near the nanotube surface. This charge cannot be easily compensated by the SWCNT due to the presence of a polymer layer on the surface of the s-SWCNTs, which is likely acting as a tunneling barrier.[96] At larger applied voltages, this separation between both on and off states becomes larger as more charge is built up at larger applied voltages.

We sought to investigate the properties of the POCB-water solid material in order to further understand the capacitance observed in the material. POCB, polymer synthesized by DuPont from renewable materials,[100] is a clear liquid with a viscosity of 325 mPa at 25°C. DuPont observed the spontaneous formation of a "gel" upon combination of water with POCB of molecular weight 510-820, but the "gel" was not characterized beyond how quickly it returned to liquid form when heated to 40°C. POCB has several close analogs: polyethylene glycol [CH_2-CH_2-O-]$_x$, polytetramethylene glycol or p(THF) [CH_2-CH_2-CH_2-CH_2-O-]$_x$, and poly(1,2-propane diol) [CH_2-CH_2(CH_3)-O-]$_x$, but none of these co-crystallize with water. This hydrate crystal structure was first observed and characterized by Tadokoro and co-workers (under the name poly(oxacyclobutane)), where molten samples of high molecular weights of POCB were quenched in ice water.[98]

POCB 650 and water form solids over a wide range of mixture compositions. With the exception of the 25 wt% water + 75 wt% POCB mixture, which appeared to be almost dry, the formed solid appeared to be either a wet paste-like solid or solid particles suspended in clear liquid. The freezing process was observed using optical microscopy. A small amount of the dry mixture described previously was placed on a microscope slide and sealed with a coverslip. The solid that formed within 2-5 minutes on the slide was composed of spherulites (Figure 20A). This morphology is typical for semicrystalline polymers and unambiguously establishes that the

solid is crystalline. In semicrystalline polymers, each spherulite normally consists of 5-30 nm thick lamellar crystals radiating outward from the center of the spherulite with amorphous regions between the lamellae[101] and the same microstructure is expected here. The spherulites appear birefringent under a polarization microscope, which is common among polymeric crystals (Figure 20B).

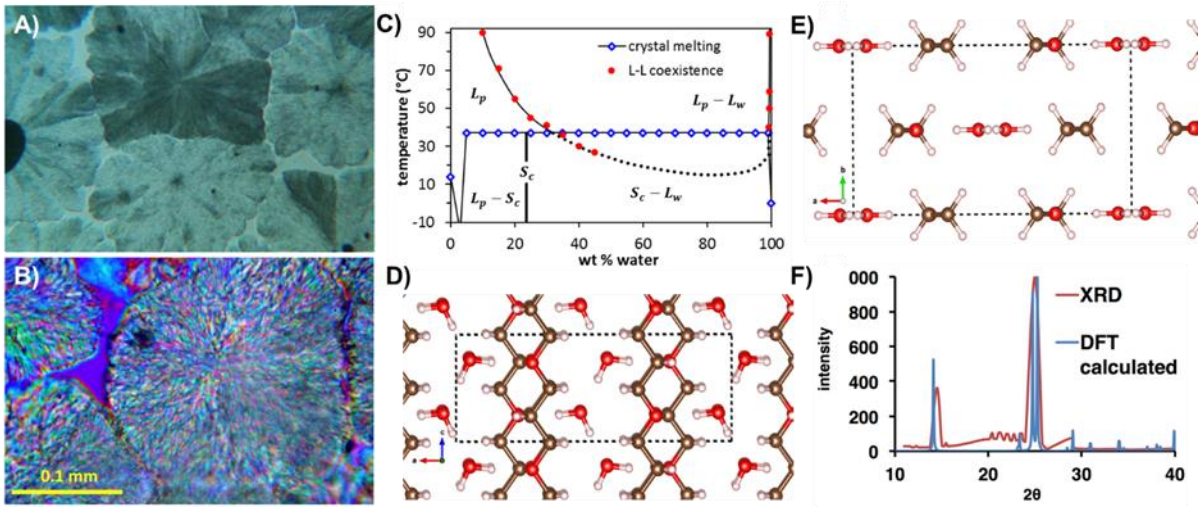

Figure 20. Characterization of POCB/water crystals. A) Optical microscope image of POCB/water spherulite crystals, indicating semi-crystalline morphology. B) Crystals under a polarization microscope showing birefringence, a common property of semi-crystalline polymer materials. C) Phase diagram of POCB/water binary mixtures at 1 atm based on L-L (liquid-liquid) phase boundary data and solid melting point data. S_c, L_p, and L_w refer to the solid co-crystal phase, polymer-rich liquid phase, and water-rich liquid phases, respectively. D) Calculated polymer hydrate structure showing aligned 1-D columns of water molecules oriented vertically. Atom color coding is as follows: carbon (brown), oxygen (red), hydrogen (white). E) A top down perspective showing 1-D aligned columns of water molecules. F) Powder X-ray diffraction (XRD) data from crystal compared with the spectrum obtained using density functional theory (DFT).

The phase behavior of POCB/water mixtures at ambient pressure was investigated utilizing cloud point data, melting point data, and an NMR-based estimate of water content in the solid crystal. A phase diagram for the binary mixture was constructed based on these experiments (Figure 20C).

Since the POCB/water solid samples are not single crystals, but polycrystalline, powder X-ray diffraction (XRD) can be expected to observe all orientations as would be observed from computationally obtained XRD spectra. Experimental powder XRD on the polycrystalline samples matched our calculated spectra from quantum chemistry modeling using the POCB hydrate structure reported by Tadokoro and co-workers.[98] Alternative POCB hydrate structures were investigated using the USPEX code[102] (Figure 20F), but these did not match the experimental XRD spectra. Calculated energy values were higher than Tadokoro's structure. The hydrate structure exhibits 1-D chains of water molecules running through the co-crystal (Figure 20D, E). We propose that these 1-D aligned channels of water molecules, which are in a hydrogen-bonded network,[98] allow for proton conductivity in POCB hydrate crystals. This type of polymer crystalline structure has been studied for proton conductivity for other polymer hydrates previously.[103] In this study, the authors found that the ionic conductivity in crystalline hydrates of linear poly(ethyleneimine) the main carriers of charge were likely protons. They found that ionic conduction in this hydrate material should primarily occur within the crystalline phases of the amorphous material and that hydrogen bonding played a critical role in the ionic conduction.[103] We have shown that POCB hydrate crystals can be capacitively charged with applied voltage bias, which is likely the result of biased proton conductivity in the material. Having the charged species near the SWCNT network electrostatically gates the nanotubes. The hysteresis observed in FET of POCB coated devices (Figure 17C) is due to the charging and discharging process of the POCB/water co-crystals lagging behind the applied gate voltage. This effect was observed for clockwise and counterclockwise I-Vg sweeps to give very similar transfer curves as is expected for this phenomenon.

3.2.1 Conclusion

In conclusion, we found that coating s-SWCNT-FET devices with POCB causes a dramatic increase in hysteresis. This hysteresis can be utilized for memory storage devices with a bit separation of ~10^4. POCB displays very interesting phase behavior and crystallizes with water at room temperature to form structures with hydrogen-bonded 1-D chains of water molecules propagating through the structure. We believe that this structure allows for trapping and shuttling of charge under applied gate bias by proton migration in the polymer crystals which is the cause of the large observed hysteresis in s-SWCNT-FET measurements. This material represents a simple and effective way to store information in nanoelectronic transistor devices. There is potential for further optimization of these devices by using high-k dielectric gate oxides (i.e., HfO_2) to improve applied voltage efficiency, allowing for lower power memory devices.

4.0 ALTERNATING CURRENT HETERODYNE MEASUREMENTS OF SWCNT DEVICES

This project focused on the building of a new instrument in our laboratory to probe our sensor devices with alternating current (AC) as opposed to direct current (DC) measurements. The signals gathered from AC heterodyne measurements have been shown to be a result of the dipole moment of the analyte interacting with the device surface (SWCNT network). This is in direct contrast with DC signals which are a result of direct charge transfer between the analyte and the sensor.

4.1 INTRODUCTION

There has been much interest in the SWCNT sensor community to develop sensors for toxic industrial gases for monitoring and alarming devices.[67] When toxic gases have not been properly monitored in the industrial setting, injury and death have resulted. Many industrial accidents that have occurred due to gas leaks could have been easily prevented and acted upon accordingly with proper monitoring devices. Unfortunately, many of these gases of concern are odorless, colorless, and toxic at very low concentrations. Detection requires accurate, fast, and sensitive sensor devices that can be installed in facilities and also worn by workers to monitor personal exposure levels. SWCNT-based devices are a great candidate for such an application because

they can be miniaturized and operate at very low power, thus not requiring workers to wear large batteries.

Two gases of great importance for industrial safety gas monitoring are hydrogen and hydrogen sulfide. Hydrogen gas is dangerous because it is a highly flammable compound and can form explosive mixtures in atmospheric air in concentrations from 4 to 74% by volume. These explosive mixtures are very easily ignited by sparks or even high temperature conditions, very common occurrences in the industrial setting. Hydrogen sulfide is toxic at very low concentrations and thus, is difficult to monitor requiring very sensitive sensor devices. OSHA has set the permissible exposure limit (PEL) of hydrogen sulfide to 10 ppm, meaning that devices that can measure at and well below that concentration are required to properly monitor hydrogen sulfide for safety.

SWCNT-based toxic gas sensors have been very thoroughly investigated in the literature due to the desire for new and improved sensing technologies.[67] Hydrogen sensing with carbon nanomaterials was first demonstrated by Kong *et al.* in 2001 using palladium decorated SWCNTs.[104] Other carbon nanomaterial-based hydrogen sensors have been developed following this work using catalytic metal nanoparticles, such as platinum, for detection.[105] The agreed upon mechanism for hydrogen sensing with these materials is catalytic splitting of hydrogen on the surface of the metal nanoparticles. It is known that these interactions on the surface of metal nanoparticles decorated on the surface of carbon nanomaterials causes a charge transfer reaction to occur with the material. This interaction is what leads to the electronic signals from metal decorated carbon nanomaterial-based sensors.[105-106] Although there are plenty of hydrogen sensors in the market, the appeal of carbon nanomaterial-based sensors is their low power operation and room temperature operation. Hydrogen sulfide sensing with carbon nanomaterials

has also been demonstrated in the literature.[107-108] These sensors take advantage of the strong binding of sulfur compounds to gold and use gold nanowires and nanoparticles to bind hydrogen sulfide. The sensor recovery from hydrogen sulfide is usually long due to the strong binding of analyte to the surface, but this can be sped up with heating.[107] Surface redox reactions have also been explored with SWCNT devices for the detection of hydrogen sulfide and can even operate in humid conditions.[109]

4.2 AC HETERODYNE INSTRUMENT SETUP

To adapt the AC heterodyne measurement method to work in our laboratory, an instrument capable of sourcing and measuring AC heterodyne signals was built. As this field is still fairly new, the setup was inferred from publications using this methodology and a synthesis of descriptions and pictures of the instrument.[70] Many improvements upon the original instrumentation in the literature were made in our adaptation of the setup. The hardware utilized for the instrument are as follows: Keithley 2400 Source Meter Unit, Keithley 3390 Arbitrary Waveform/Function Generator, Stanford Research Systems SR 830 Lock-In Amplifier. The instruments were operated from a computer running a custom LabView program through GPIB communication.

4.2.1 Hardware Wiring and Setup

Utilizing all of the hardware described previously, the setup shown in Figure 13B was wired together using BNC cables and an appropriate bias tee to protect both the DC and AC sources

used in the setup. All outer sleeves of the BNC cables were grounded and the SWCNT devices were measured with a shielded device probing station. All instruments were operated with a custom program written in Labview 2011.

4.2.2 SWCNT Device Preparation

The semiconducting SWCNTs used in this work were 99.99% Isosol S100 in toluene (0.01 mg/mL). s-SWCNT devices used in this work were fabricated by dielectrophoretic deposition (100 kH, 10 V_{pp}, 90 sec) of this solution onto pre-fabricated interdigitated gold finger devices. Two different sensor chemistries were utilized in this work, platinum and palladium nanoparticle-decorated s-SWCNTs. In the course of this project, we discovered that polymer coated s-SWCNTs can seed metal nanoparticles on their surface (Figure 21).

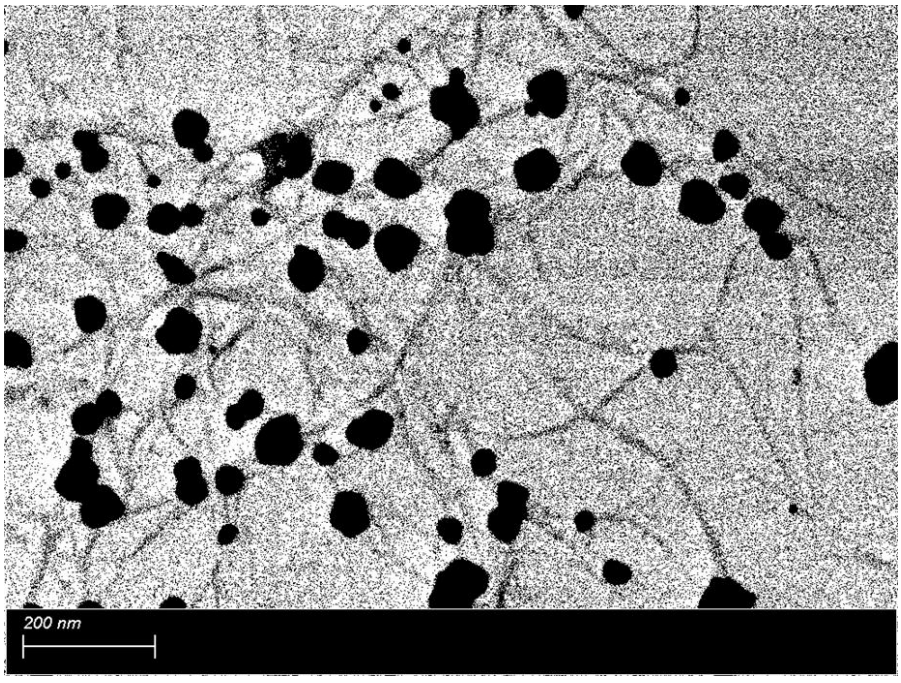

Figure 21. SEM image of gold nanoparticle decorated Isosol S100 SWCNTs after 10s deposition. All nanoparticles are associated with the sidewall of the s-SWCNTs and vary in size and morphology. Image color thresholds were adjusted in ImageJ for clarity.

Metal nanoparticles were deposited on devices by bulk electrolysis of two different metal salt solutions in 0.1 M HCl ($Pd(acac)_2$, and $PtCl_4$, 1 mM) with the s-SWCNT device as the working electrode, Ag/AgCl as the reference, and Pt wire as the counter. The electrolysis voltage used was -0.3 V applied for 10 seconds on each device.

4.3 AC HETERODYNE MEASUREMENTS

The AC heterodyne setup was used to measure hydrogen and hydrogen sulfide gases. The platinum nanoparticle (Pt-NP) decorated s-SWCNT devices were used for hydrogen sulfide sensing due to better recovery times. Sensing still occurs because the electrodes are made of gold. Palladium nanoparticle (Pd-NP) decorated devices were used for hydrogen sensing as this is a widely used metal for this application. We hypothesized that with a DC FET measurement, we would observe charge transfer to the s-SWCNT devices in both cases. This would result in a decrease in conductance upon exposure to either hydrogen sulfide or hydrogen gas. The AC heterodyne setup detects molecular dipoles and is completely insensitive to charge transfer reactions. It is expected that if the same sensor devices are exposed to hydrogen and hydrogen sulfide gas, the AC measurement should not change when exposed to hydrogen gas, but would still change when exposed to hydrogen sulfide due to its large dipole moment.

4.3.1 DC Sensor Measurements

The direct current measurements were taken with 2 Keithley 2400 Sourcemeters. The devices were addressed through a custom built 40-pin ZIF breakout board. The Sourcemeters were

operated from a custom program written in LabView 2011 to source a constant bias between source and drain electrodes (50 mV) while measuring drain current (I_d) and sweep gate voltage (V_g) in a triangle wave pattern. The gate voltage was swept from +20 V to -20 V back to +20 V in 200 total steps to get a profile of the transfer curve and its hysteresis. The output data for the DC measurements is an I_d vs. V_g plot, the FET transfer curve.

4.3.2 AC Heterodyne Sensor Measurements

The AC heterodyne measurements were taken with the instruments and setup described previously in section 4.2 to 4.2.1. The bias between source and drain electrodes was set to 25 mVAC at 100 kHz modulated with 1.234 kHz frequency. The gate voltage was applied using a Keithley 2400 Sourcemeter with drain referenced to source through a bias tee. The mixing current at 1.234 kHz was measured with an SR 830 Lock In Amplifier with 10^6 amplification in current mode. The mixing current (I_{mix}) was plotted vs. V_g as the output.

4.3.3 Gas Delivery System

Analyte gases were delivered with nitrogen as a carrier gas. Stock tanks of 100 ppm hydrogen sulfide (balanced in nitrogen) and 100 ppm hydrogen (balanced in nitrogen) were diluted with nitrogen carrier gas to 25 ppm. The total flow rate was always kept at 200 sccm. The devices were contained in a custom-built Teflon flow chamber where they were exposed to the gas flows. Before any measurements were taken, the devices were dried under nitrogen for 20 minutes. A nitrogen blank was taken for all devices, then the flow was switched to 25 ppm analyte gas by properly diluting with nitrogen carrier gas. The analyte gas was allowed to flow over the devices

for 3 minutes before measurements were taken to ensure that the sensors were at maximum signal.

4.3.4 AC vs. DC Sensing Results

Two sets of Pd-NP and Pt-NP decorated devices were fabricated as described and exposed to hydrogen and hydrogen sulfide gas (25 ppm) as described. FET measurements were taken both for the blanks (nitrogen gas) and after 3 minute exposures to analyte gas at 25 ppm. The measurement results are displayed in Figure 22.

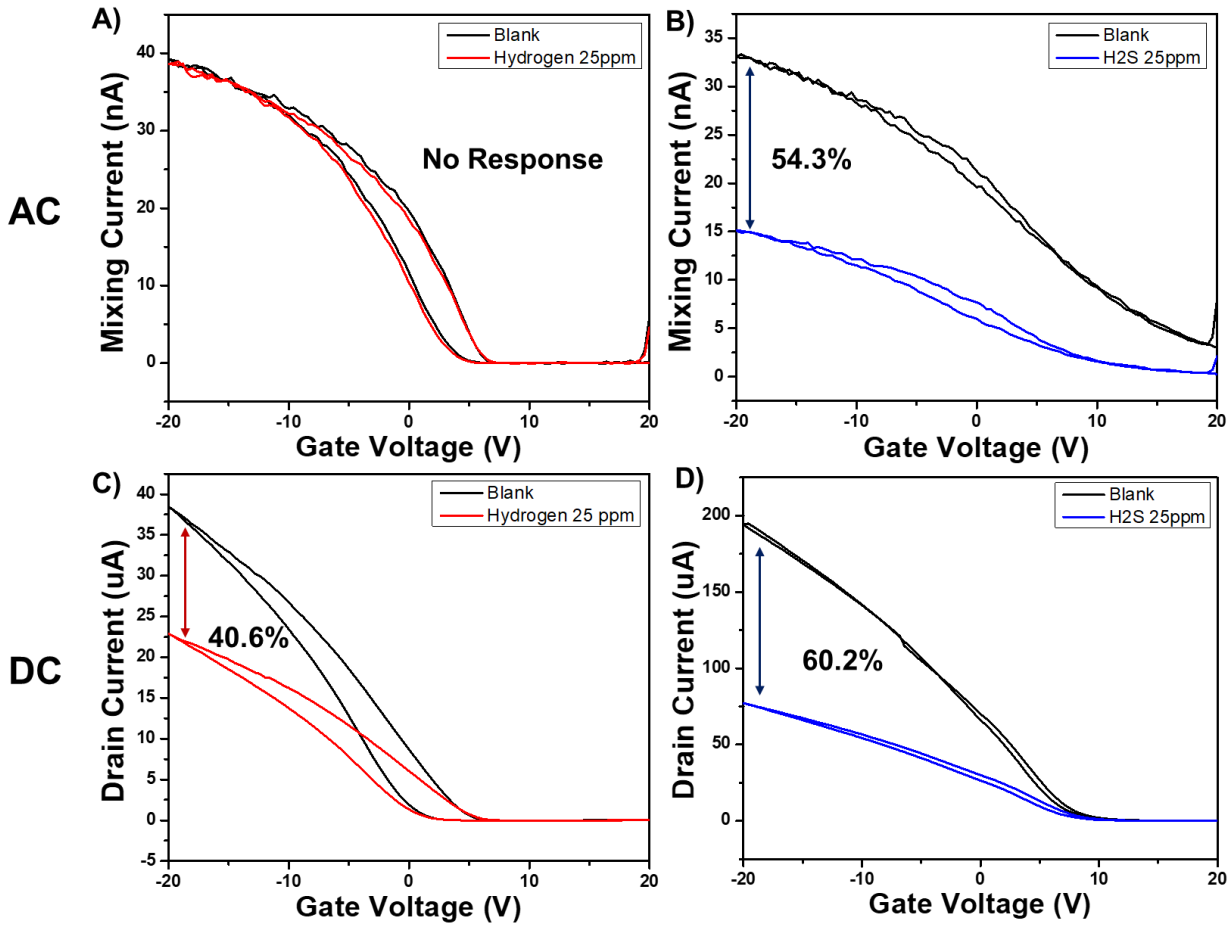

Figure 22. AC heterodyne versus DC FET sensing for hydrogen and hydrogen sulfide gas with palladium and platinum nanoparticle decorated s-SWCNTs, respectively. A) No response to hydrogen was observed in AC due to the lack of a dipole in hydrogen gas. B) A decrease in mixing current was observed in AC due to the strong dipole moment of hydrogen sulfide. C) A strong response to hydrogen gas was observed in DC as was expected for this material. C) A strong response to hydrogen sulfide was observed in DC, also as expected for this material.

The results confirm the initial hypothesis that hydrogen does not show any noticeable signal (above noise levels) (Figure 22A) and this same sensor shows a very large response to hydrogen in DC FET measurements (Figure 22C). The AC and DC sensors both responded to hydrogen sulfide gas due to its large dipole moment (Figure 22B) and its strong binding and charge transfer interaction with the s-SWCNTs.

In this work, it was shown that s-SWCNT sensors can be used for direct current and alternating current measurements by simply changing how voltage is sourced and the signal is measured. AC heterodyne opens up many possibilities in the world of vapor sensing as it can be used to differentiate between molecules with and without dipoles. When coupled with standard DC measurements, a very powerful sensing tool is realized with wide ranging applications in gas sensing of toxic and flammable gases. Many other aspects of AC heterodyne gas sensing have yet to be explored, but it is a new promising and actively growing field.

Bibliography

1. Iijima, S., Helical microtubules of graphitic carbon. *Nature (London)* **1991,** *354* (6348), 56-8.

2. Tans, S. J.; Verschueren, A. R. M.; Dekker, C., Room-temperature transistor based on a single carbon nanotube. *Nature* **1998,** *393* (6680), 49-52.

3. Davenport, M., Twists and Shouts: A Nanotube Story. *Chem. Eng. News* June 8, 2013, 2015, pp 10-15.

4. Vijayaraghavan, A.; Hennrich, F.; Stürzl, N.; Engel, M.; Ganzhorn, M.; Oron-Carl, M.; Marquardt, C. W.; Dehm, S.; Lebedkin, S.; Kappes, M. M.; Krupke, R., Toward Single-Chirality Carbon Nanotube Device Arrays. *ACS Nano* **2010,** *4* (5), 2748-2754.

5. Ganzhorn, M.; Vijayaraghavan, A.; Dehm, S.; Hennrich, F.; Green, A. A.; Fichtner, M.; Voigt, A.; Rapp, M.; von Löhneysen, H.; Hersam, M. C.; Kappes, M. M.; Krupke, R., Hydrogen Sensing with Diameter- and Chirality-Sorted Carbon Nanotubes. *ACS Nano* **2011,** *5* (3), 1670-1676.

6. Lee, D.; Lee, B. H.; Yoon, J.; Ahn, D. C.; Park, J. Y.; Hur, J.; Kim, M. S.; Jeon, S. B.; Kang, M. H.; Kim, K.; Lim, M.; Choi, S. J.; Choi, Y. K., Three-Dimensional Fin-Structured Semiconducting Carbon Nanotube Network Transistor. *ACS Nano* **2016,** *10* (12), 10894-10900.

7. Cao, Q.; Han, S. J.; Tulevski, G. S., Fringing-field dielectrophoretic assembly of ultrahigh-density semiconducting nanotube arrays with a self-limited pitch. *Nat. Commun.* **2014,** *5*, 5071.

8. Bronikowski, M. J.; Willis, P. A.; Colbert, D. T.; Smith, K. A.; Smalley, R. E., Gas-phase production of carbon single-walled nanotubes from carbon monoxide via the HiPco process: A parametric study. *J. Vac. Sci. Technol., A* **2001,** *19* (4), 1800-1805.

9. Kroto, H. W.; Heath, J. R.; O'Brien, S. C.; Curl, R. F.; Smalley, R. E., C60: Buckminsterfullerene. *Nature* **1985,** *318* (6042), 162-163.

10. Flahaut, E.; Peigney, A.; Laurent, C.; Rousset, A., Synthesis of single-walled carbon nanotube-Co-MgO composite powders and extraction of the nanotubes. *J. Mater. Chem.* **2000,** *10* (2), 249-252.

11. Novoselov, K. S.; Geim, A. K.; Morozov, S. V.; Jiang, D.; Zhang, Y.; Dubonos, S. V.; Grigorieva, I. V.; Firsov, A. A., Electric Field Effect in Atomically Thin Carbon Films. *Science* **2004,** *306* (5696), 666-669.

12. Geim, A. K.; Novoselov, K. S., The rise of graphene. *Nat. Mater.* **2007,** *6* (3), 183-191.

13. Saito, R. D., G.; Dresselhaus, M.S., *Physical Properties of Carbon Nanotubes*. World Scientific: Singapore: 1998.

14. Hitosugi, S.; Nakanishi, W.; Yamasaki, T.; Isobe, H., Bottom-up synthesis of finite models of helical (n,m)-single-wall carbon nanotubes. *Nat. Commun.* **2011,** *2*, 492.

15. Zheng, L. X.; O'Connell, M. J.; Doorn, S. K.; Liao, X. Z.; Zhao, Y. H.; Akhadov, E. A.; Hoffbauer, M. A.; Roop, B. J.; Jia, Q. X.; Dye, R. C.; Peterson, D. E.; Huang, S. M.; Liu, J.; Zhu, Y. T., Ultralong single-wall carbon nanotubes. *Nat. Mater.* **2004,** *3* (10), 673-676.

16. Arnold, M. S.; Green, A. A.; Hulvat, J. F.; Stupp, S. I.; Hersam, M. C., Sorting carbon nanotubes by electronic structure using density differentiation. *Nat. Nanotechnol.* **2006,** *1* (1), 60-65.

17. Liu, H. P.; Nishide, D.; Tanaka, T.; Kataura, H., Large-scale single-chirality separation of single-wall carbon nanotubes by simple gel chromatography. *Nat. Commun.* **2011,** *2*, 309.

18. Wilder, J. W. G.; Venema, L. C.; Rinzler, A. G.; Smalley, R. E.; Dekker, C., Electronic structure of atomically resolved carbon nanotubes. *Nature* **1998,** *391* (6662), 59-62.

19. Hodge, S. A.; Bayazit, M. K.; Coleman, K. S.; Shaffer, M. S. P., Unweaving the rainbow: a review of the relationship between single-walled carbon nanotube molecular structures and their chemical reactivity. *Chem. Soc. Rev.* **2012,** *41* (12), 4409-4429.

20. Jorio, A.; Saito, R.; Hafner, J. H.; Lieber, C. M.; Hunter, M.; McClure, T.; Dresselhaus, G.; Dresselhaus, M. S., Structural Determination of Isolated Single-Wall Carbon Nanotubes by Resonant Raman Scattering. *Phys. Rev. Lett.* **2001,** *86* (6), 1118-1121.

21. Fantini, C.; Jorio, A.; Souza, M.; Strano, M. S.; Dresselhaus, M. S.; Pimenta, M. A., Optical Transition Energies for Carbon Nanotubes from Resonant Raman Spectroscopy: Environment and Temperature Effects. *Phys. Rev. Lett.* **2004,** *93* (14), 147406.

22. Kataura, H.; Kumazawa, Y.; Maniwa, Y.; Umezu, I.; Suzuki, S.; Ohtsuka, Y.; Achiba, Y., Optical properties of single-wall carbon nanotubes. *Synthetic Metals* **1999,** *103* (1–3), 2555-2558.

23. Bachilo, S. M.; Strano, M. S.; Kittrell, C.; Hauge, R. H.; Smalley, R. E.; Weisman, R. B., Structure-Assigned Optical Spectra of Single-Walled Carbon Nanotubes. *Science* **2002,** *298* (5602), 2361-2366.

24. Weisman, R. B.; Bachilo, S. M., Dependence of Optical Transition Energies on Structure for Single-Walled Carbon Nanotubes in Aqueous Suspension: An Empirical Kataura Plot. *Nano Lett.* **2003,** *3* (9), 1235-1238.

25. Naumov, A. V.; Ghosh, S.; Tsyboulski, D. A.; Bachilo, S. M.; Weisman, R. B., Analyzing Absorption Backgrounds in Single-Walled Carbon Nanotube Spectra. *ACS Nano* **2011,** *5* (3), 1639-1648.

26. O'Connell, M. J.; Bachilo, S. M.; Huffman, C. B.; Moore, V. C.; Strano, M. S.; Haroz, E. H.; Rialon, K. L.; Boul, P. J.; Noon, W. H.; Kittrell, C.; Ma, J.; Hauge, R. H.; Weisman, R. B.; Smalley, R. E., Band Gap Fluorescence from Individual Single-Walled Carbon Nanotubes. *Science* **2002,** *297* (5581), 593-596.

27. Tabakman, S. M.; Welsher, K.; Hong, G.; Dai, H., Optical Properties of Single-Walled Carbon Nanotubes Separated in a Density Gradient; Length, Bundling, and Aromatic Stacking Effects. *J. Phys. Chem. C* **2010,** *114* (46), 19569-19575.

28. Shigeo, M.; Yuhei, M.; Yoichi, M.; Shohei, C., Optical characterization of single-walled carbon nanotubes synthesized by catalytic decomposition of alcohol. *New J. Phys.* **2003,** *5* (1), 149.

29. Dresselhaus, M. S.; Dresselhaus, G.; Saito, R.; Jorio, A., Raman spectroscopy of carbon nanotubes. *Phys. Rep.* **2005,** *409* (2), 47-99.

30. Jovanovic, S. P.; Markovic, Z. M.; Kleut, D. N.; Dramicanin, M. D.; Holclajtner-Antunovic, I. D.; Milosavljevic, M. S.; La Parola, V.; Syrgiannis, Z.; Markovic, B. M. T., Structural Analysis of Single Wall Carbon Nanotubes Exposed to Oxidation and Reduction Conditions in the Course of Gamma Irradiation. *J. Phys. Chem. C* **2014,** *118* (29), 16147-16155.

31. Kane, A. A.; Ford, A. C.; Nissen, A.; Krafcik, K. L.; Leonard, F., Etching of Surfactant from Solution-Processed, Type-Separated Carbon Nanotubes and Impact on Device Behavior. *ACS Nano* **2014,** *8* (3), 2477-2485.

32. Corio, P.; Santos, P. S.; Brar, V. W.; Samsonidze, G. G.; Chou, S. G.; Dresselhaus, M. S., Potential dependent surface Raman spectroscopy of single wall carbon nanotube films on platinum electrodes. *Chem. Phys. Lett.* **2003,** *370* (5–6), 675-682.

33. Li, J.; Ke, C.-T.; Liu, K.; Li, P.; Liang, S.; Finkelstein, G.; Wang, F.; Liu, J., Importance of Diameter Control on Selective Synthesis of Semiconducting Single-Walled Carbon Nanotubes. *ACS Nano* **2014,** *8* (8), 8564-8572.

34. Yang, F.; Wang, X.; Zhang, D.; Yang, J.; LuoDa; Xu, Z.; Wei, J.; Wang, J.-Q.; Xu, Z.; Peng, F.; Li, X.; Li, R.; Li, Y.; Li, M.; Bai, X.; Ding, F.; Li, Y., Chirality-specific growth

of single-walled carbon nanotubes on solid alloy catalysts. *Nature* **2014,** *510* (7506), 522-524.

35. Liu, J.; Wang, C.; Tu, X. M.; Liu, B. L.; Chen, L.; Zheng, M.; Zhou, C. W., Chirality-controlled synthesis of single-wall carbon nanotubes using vapour-phase epitaxy. *Nat. Commun.* **2012,** *3*, 7.

36. Liu, B. L.; Liu, J.; Tu, X. M.; Zhang, J. L.; Zheng, M.; Zhou, C. W., Chirality-Dependent Vapor-Phase Epitaxial Growth and Termination of Single-Wall Carbon Nanotubes. *Nano Lett.* **2013,** *13* (9), 4416-4421.

37. Arnold, M. S.; Green, A. A.; Hulvat, J. F.; Stupp, S. I.; Hersam, M. C., Sorting carbon nanotubes by electronic structure using density differentiation. *Nat. Nanotechnol.* **2006,** *1* (1), 60-65.

38. Green, A. A.; Hersam, M. C., Nearly single-chirality single-walled carbon nanotubes produced via orthogonal iterative density gradient ultracentrifugation. *Adv. Mater.* **2011,** *23* (19), 2185-90.

39. Arnold, M. S.; Stupp, S. I.; Hersam, M. C., Enrichment of Single-Walled Carbon Nanotubes by Diameter in Density Gradients. *Nano Lett.* **2005,** *5* (4), 713-718.

40. Tvrdy, K.; Jain, R. M.; Han, R.; Hilmer, A. J.; McNicholas, T. P.; Strano, M. S., A Kinetic Model for the Deterministic Prediction of Gel-Based Single-Chirality Single-Walled Carbon Nanotube Separation. *Acs Nano* **2013,** *7* (2), 1779-1789.

41. Nish, A.; Hwang, J. Y.; Doig, J.; Nicholas, R. J., Highly selective dispersion of single-walled carbon nanotubes using aromatic polymers. *Nat. Nanotechnol.* **2007,** *2* (10), 640-646.

42. Lee, H. W.; Yoon, Y.; Park, S.; Oh, J. H.; Hong, S.; Liyanage, L. S.; Wang, H.; Morishita, S.; Patil, N.; Park, Y. J.; Park, J. J.; Spakowitz, A.; Galli, G.; Gygi, F.; Wong, P. H.; Tok, J. B.; Kim, J. M.; Bao, Z., Selective dispersion of high purity semiconducting single-walled carbon nanotubes with regioregular poly(3-alkylthiophene)s. *Nat. Commun.* **2011,** *2*, 541.

43. Hwang, J. Y.; Nish, A.; Doig, J.; Douven, S.; Chen, C. W.; Chen, L. C.; Nicholas, R. J., Polymer structure and solvent effects on the selective dispersion of single-walled carbon nanotubes. *J. Am. Chem. Soc.* **2008,** *130* (11), 3543-53.

44. Clar, J. G.; Silvera Batista, C. A.; Youn, S.; Bonzongo, J.-C. J.; Ziegler, K. J., Interactive Forces between Sodium Dodecyl Sulfate-Suspended Single-Walled Carbon Nanotubes and Agarose Gels. *J. Am. Chem. Soc.* **2013,** *135* (47), 17758-17767.

45. Clar, J. G.; Yuan, T. Y.; Zhao, Y.; Bonzongo, J. C. J.; Ziegler, K. J., Evaluation of Critical Parameters in the Separation of Single-Wall Carbon Nanotubes through Selective Adsorption onto Hydrogels. *J. Phys. Chem. C* **2014,** *118* (28), 15495-15505.

46. Jain, R. M.; Tvrdy, K.; Han, R.; Ulissi, Z.; Strano, M. S., Quantitative Theory of Adsorptive Separation for the Electronic Sorting of Single-Walled Carbon Nanotubes. *Acs Nano* **2014,** *8* (4), 3367-3379.

47. Tummala, N. R.; Striolo, A., Curvature effects on the adsorption of aqueous sodium-dodecyl-sulfate surfactants on carbonaceous substrates: Structural features and counterion dynamics. *Phys. Rev. E* **2009,** *80* (2), 021408.

48. Zhou, X.; Park, J. Y.; Huang, S.; Liu, J.; McEuen, P. L., Band structure, phonon scattering, and the performance limit of single-walled carbon nanotube transistors. *Phys. Rev. Lett.* **2005,** *95* (14), 146805.

49. Ding, J.; Li, Z.; Lefebvre, J.; Cheng, F.; Dubey, G.; Zou, S.; Finnie, P.; Hrdina, A.; Scoles, L.; Lopinski, G. P.; Kingston, C. T.; Simard, B.; Malenfant, P. R. L., Enrichment of large-diameter semiconducting SWCNTs by polyfluorene extraction for high network density thin film transistors. *Nanoscale* **2014,** *6* (4), 2328-2339.

50. Lilienfeld, J. E. Method and Apparatus for Controlling Electric Current. 1926.

51. White, C. T.; Todorov, T. N., Carbon nanotubes as long ballistic conductors. *Nature* **1998,** *393* (6682), 240-242.

52. Franklin, A. D.; Luisier, M.; Han, S.-J.; Tulevski, G.; Breslin, C. M.; Gignac, L.; Lundstrom, M. S.; Haensch, W., Sub-10 nm Carbon Nanotube Transistor. *Nano Lett.* **2012,** *12* (2), 758-762.

53. Cao, Q.; Rogers, J. A., Ultrathin Films of Single-Walled Carbon Nanotubes for Electronics and Sensors: A Review of Fundamental and Applied Aspects. *Adv. Mater.* **2009,** *21* (1), 29-53.

54. Shimizu, M.; Fujii, S.; Tanaka, T.; Kataura, H., Effects of Surfactants on the Electronic Transport Properties of Thin-Film Transistors of Single-Wall Carbon Nanotubes. *J. Phys. Chem. C* **2013,** *117* (22), 11744-11749.

55. Zhang, Z. B.; Cardenas, J.; Campbell, E. E. B.; Zhang, S. L., Reversible surface functionalization of carbon nanotubes for fabrication of field-effect transistors. *Appl. Phys. Lett.* **2005,** *87* (4), 043110.

56. Wang, J.; Sun, J.; Gao, L.; Wang, Y.; Zhang, J.; Kajiura, H.; Li, Y.; Noda, K., Removal of the Residual Surfactants in Transparent and Conductive Single-Walled Carbon Nanotube Films. *The Journal of Physical Chemistry C* **2009,** *113* (41), 17685-17690.

57. Fu, Q.; Liu, J., Effects of Ionic Surfactant Adsorption on Single-Walled Carbon Nanotube Thin Film Devices in Aqueous Solutions. *Langmuir* **2005,** *21* (4), 1162-1165.

58. Fuhrer, M. S.; Nygård, J.; Shih, L.; Forero, M.; Yoon, Y.-G.; Mazzoni, M. S. C.; Choi, H. J.; Ihm, J.; Louie, S. G.; Zettl, A.; McEuen, P. L., Crossed Nanotube Junctions. *Science* **2000,** *288* (5465), 494-497.

59. Engel, M.; Small, J. P.; Steiner, M.; Freitag, M.; Green, A. A.; Hersam, M. C.; Avouris, P., Thin Film Nanotube Transistors Based on Self-Assembled, Aligned, Semiconducting Carbon Nanotube Arrays. *ACS Nano* **2008,** *2* (12), 2445-2452.

60. Shekhar, S.; Stokes, P.; Khondaker, S. I., Ultrahigh Density Alignment of Carbon Nanotube Arrays by Dielectrophoresis. *ACS Nano* **2011,** *5* (3), 1739-1746.

61. Qian, Q.; Li, G.; Jin, Y.; Liu, J.; Zou, Y.; Jiang, K.; Fan, S.; Li, Q., Trap-State-Dominated Suppression of Electron Conduction in Carbon Nanotube Thin-Film Transistors. *ACS Nano* **2014,** *8* (9), 9597-9605.

62. Kim, W.; Javey, A.; Vermesh, O.; Wang, Q.; Li, Y.; Dai, H., Hysteresis Caused by Water Molecules in Carbon Nanotube Field-Effect Transistors. *Nano Lett.* **2003,** *3* (2), 193-198.

63. Franklin, A. D., Electronics: The road to carbon nanotube transistors. *Nature* **2013,** *498* (7455), 443-444.

64. Jin, S. H.; Dunham, S. N.; Song, J.; Xie, X.; Kim, J.-h.; Lu, C.; Islam, A.; Du, F.; Kim, J.; Felts, J.; Li, Y.; Xiong, F.; Wahab, M. A.; Menon, M.; Cho, E.; Grosse, K. L.; Lee, D. J.; Chung, H. U.; Pop, E.; Alam, M. A.; King, W. P.; Huang, Y.; Rogers, J. A., Using nanoscale thermocapillary flows to create arrays of purely semiconducting single-walled carbon nanotubes. *Nat. Nanotechnol.* **2013,** *8* (5), 347-355.

65. Cinke, M.; Li, J.; Chen, B.; Cassell, A.; Delzeit, L.; Han, J.; Meyyappan, M., Pore structure of raw and purified HiPco single-walled carbon nanotubes. *Chem. Phys. Lett.* **2002,** *365* (1–2), 69-74.

66. Sorgenfrei, S.; Chiu, C.-y.; Gonzalez, R. L.; Yu, Y.-J.; Kim, P.; Nuckolls, C.; Shepard, K. L., Label-free single-molecule detection of DNA-hybridization kinetics with a carbon nanotube field-effect transistor. *Nat. Nanotechnol.* **2011,** *6* (2), 126-132.

67. Kauffman, D. R.; Star, A., Carbon Nanotube Gas and Vapor Sensors. *Angew. Chem., Int. Ed.* **2008,** *47* (35), 6550-6570.

68. Heller, I.; Janssens, A. M.; Männik, J.; Minot, E. D.; Lemay, S. G.; Dekker, C., Identifying the Mechanism of Biosensing with Carbon Nanotube Transistors. *Nano Lett.* **2008,** *8* (2), 591-595.

69. Zhang, L.; Tu, X.; Welsher, K.; Wang, X.; Zheng, M.; Dai, H., Optical Characterizations and Electronic Devices of Nearly Pure (10,5) Single-Walled Carbon Nanotubes. *J. Am. Chem. Soc.* **2009,** *131* (7), 2454-2455.

70. Kulkarni, G. S.; Zang, W.; Zhong, Z., Nanoelectronic Heterodyne Sensor: A New Electronic Sensing Paradigm. *Acc. Chem. Res.* **2016,** *49* (11), 2578-2586.

71. Kumar, B.; Min, K.; Bashirzadeh, M.; Farimani, A. B.; Bae, M. H.; Estrada, D.; Kim, Y. D.; Yasaei, P.; Park, Y. D.; Pop, E.; Aluru, N. R.; Salehi-Khojin, A., The Role of

External Defects in Chemical Sensing of Graphene Field-Effect Transistors. *Nano Lett.* **2013,** *13* (5), 1962-1968.

72. Dan, Y.; Lu, Y.; Kybert, N. J.; Luo, Z.; Johnson, A. T. C., Intrinsic Response of Graphene Vapor Sensors. *Nano Lett.* **2009,** *9* (4), 1472-1475.

73. Kulkarni, G. S.; Zhong, Z., Detection beyond the Debye screening length in a high-frequency nanoelectronic biosensor. *Nano Lett.* **2012,** *12* (2), 719-723.

74. Kulkarni, G. S.; Zhong, Z., Fabrication of carbon nanotube high-frequency nanoelectronic biosensor for sensing in high ionic strength solutions. *J. Vis. Exp.* **2013,** (77).

75. Kulkarni, G. S.; Reddy, K.; Zhong, Z.; Fan, X., Graphene nanoelectronic heterodyne sensor for rapid and sensitive vapour detection. *Nat. Commun.* **2014,** *5*, 4376.

76. Kulkarni, G. S.; Reddy, K.; Zang, W.; Lee, K.; Fan, X.; Zhong, Z., Electrical Probing and Tuning of Molecular Physisorption on Graphene. *Nano Lett.* **2016,** *16* (1), 695-700.

77. Star, A.; Han, T.-R.; Gabriel, J.-C. P.; Bradley, K.; Grüner, G., Interaction of Aromatic Compounds with Carbon Nanotubes: Correlation to the Hammett Parameter of the Substituent and Measured Carbon Nanotube FET Response. *Nano Lett.* **2003,** *3* (10), 1421-1423.

78. Ortiz-Conde, A.; García Sánchez, F. J.; Liou, J. J.; Cerdeira, A.; Estrada, M.; Yue, Y., A review of recent MOSFET threshold voltage extraction methods. *Microelectron. Reliab.* **2002,** *42* (4–5), 583-596.

79. Javey, A.; Guo, J.; Wang, Q.; Lundstrom, M.; Dai, H., Ballistic carbon nanotube field-effect transistors. *Nature* **2003,** *424* (6949), 654-657.

80. Iijima, S., Helical microtubules of graphitic carbon. *Nature* **1991,** *354* (6348), 56-58.

81. Treacy, M. M. J.; Ebbesen, T. W.; Gibson, J. M., Exceptionally high Young's modulus observed for individual carbon nanotubes. *Nature* **1996,** *381* (6584), 678-680.

82. Münzer, A. M.; Michael, Z. P.; Star, A., Carbon Nanotubes for the Label-Free Detection of Biomarkers. *ACS Nano* **2013,** *7* (9), 7448-7453.

83. Sun, D.-m.; Timmermans, M. Y.; Tian, Y.; Nasibulin, A. G.; Kauppinen, E. I.; Kishimoto, S.; Mizutani, T.; Ohno, Y., Flexible high-performance carbon nanotube integrated circuits. *Nat. Nanotechnol.* **2011,** *6* (3), 156-161.

84. Cao, Q.; Kim, H.-s.; Pimparkar, N.; Kulkarni, J. P.; Wang, C.; Shim, M.; Roy, K.; Alam, M. A.; Rogers, J. A., Medium-scale carbon nanotube thin-film integrated circuits on flexible plastic substrates. *Nature* **2008,** *454* (7203), 495-500.

85. Fuhrer, M. S.; Kim, B. M.; Dürkop, T.; Brintlinger, T., High-Mobility Nanotube Transistor Memory. *Nano Lett.* **2002,** *2* (7), 755-759.

86. Rinkiö, M.; Johansson, A.; Paraoanu, G. S.; Törmä, P., High-Speed Memory from Carbon Nanotube Field-Effect Transistors with High-κ Gate Dielectric. *Nano Lett.* **2009,** *9* (2), 643-647.

87. Star, A.; Lu, Y.; Bradley, K.; Grüner, G., Nanotube Optoelectronic Memory Devices. *Nano Lett.* **2004,** *4* (9), 1587-1591.

88. Rueckes, T.; Kim, K.; Joselevich, E.; Tseng, G. Y.; Cheung, C.-L.; Lieber, C. M., Carbon Nanotube-Based Nonvolatile Random Access Memory for Molecular Computing. *Science* **2000,** *289* (5476), 94.

89. Collins, P. G.; Arnold, M. S.; Avouris, P., Engineering Carbon Nanotubes and Nanotube Circuits Using Electrical Breakdown. *Science* **2001,** *292* (5517), 706.

90. Zhang, G.; Qi, P.; Wang, X.; Lu, Y.; Li, X.; Tu, R.; Bangsaruntip, S.; Mann, D.; Zhang, L.; Dai, H., Selective Etching of Metallic Carbon Nanotubes by Gas-Phase Reaction. *Science* **2006,** *314* (5801), 974.

91. Javey, A.; Guo, J.; Farmer, D. B.; Wang, Q.; Wang, D.; Gordon, R. G.; Lundstrom, M.; Dai, H., Carbon Nanotube Field-Effect Transistors with Integrated Ohmic Contacts and High-κ Gate Dielectrics. *Nano Lett.* **2004,** *4* (3), 447-450.

92. Derycke, V.; Martel, R.; Appenzeller, J.; Avouris, P., Controlling doping and carrier injection in carbon nanotube transistors. *Appl. Phys. Lett.* **2002,** *80* (15), 2773.

93. Radosavljević, M.; Freitag, M.; Thadani, K. V.; Johnson, A. T., Nonvolatile Molecular Memory Elements Based on Ambipolar Nanotube Field Effect Transistors. *Nano Lett.* **2002,** *2* (7), 761-764.

94. Di Bartolomeo, A.; Rinzan, M.; Boyd, A. K.; Yang, Y.; Guadagno, L.; Giubileo, F.; Barbara, P., Electrical properties and memory effects of field-effect transistors from networks of single- and double-walled carbon nanotubes. *Nanotechnology* **2010,** *21* (11), 115204.

95. Cho, B.; Kim, K.; Chen, C.-L.; Shen, A. M.; Truong, Q.; Chen, Y., Nonvolatile Analog Memory Transistor Based on Carbon Nanotubes and C60 Molecules. *Small* **2013,** *9* (13), 2283-2287.

96. Hwang, I.; Wang, W.; Hwang, S. K.; Cho, S. H.; Kim, K. L.; Jeong, B.; Huh, J.; Park, C., Multilevel non-volatile data storage utilizing common current hysteresis of networked single walled carbon nanotubes. *Nanoscale* **2016,** *8* (19), 10273-10281.

97. Di Bartolomeo, A.; Yang, Y.; Rinzan, M. B. M.; Boyd, A. K.; Barbara, P., Record Endurance for Single-Walled Carbon Nanotube–Based Memory Cell. *Nanoscale Res. Lett.* **2010,** *5* (11), 1852.

98. Kakida, H.; Makino, D.; Chatani, Y.; Kobayashi, M.; Tadokoro, H., Strutural Studies of Polyethers [-(CH2)mO-]n. VIII. Polyoxacyclobutane Hydrate (Modification I). *Macromolecules* **1970,** *3* (5), 569-578.

99. Ding, J.; Li, Z.; Lefebvre, J.; Cheng, F.; Dunford, J. L.; Malenfant, P. R. L.; Humes, J.; Kroeger, J., A hybrid enrichment process combining conjugated polymer extraction and silica gel adsorption for high purity semiconducting single-walled carbon nanotubes (SWCNT). *Nanoscale* **2015,** *7* (38), 15741-15747.

100. Harmer, M. A.; Confer, D. C.; Hoffman, C. K.; Jackson, S. C.; Liauw, A. Y.; Minter, A. R.; Murphy, E. R.; Spence, R. E.; Sunkara, H. B., Renewably sourced polytrimethylene ether glycol by superacid catalyzed condensation of 1,3-propanediol. *Green Chem.* **2010,** *12* (8), 1410.

101. Hiemenz, P. C.; Lodge, T. P., Chapter 13: Crystalline Polymers. In *Polymer Chemistry*, CRC Press: Boca Raton, 2007; p 511.

102. Zhu, Q.; Sharma, V.; Oganov, A. R.; Ramprasad, R., Predicting polymeric crystal structures by evolutionary algorithms. *J. Chem. Phys.* **2014,** *141* (15), 154102.

103. Watanabe, M.; Ikezawa, R.; Sanui, K.; Ogata, N., Protonic conduction in poly(ethylenimine) hydrates. *Macromolecules* **1987,** *20* (5), 968-973.

104. Kong, J.; Chapline, M. G.; Dai, H., Functionalized Carbon Nanotubes for Molecular Hydrogen Sensors. *Adv. Mater.* **2001,** *13* (18), 1384-1386.

105. Vedala, H.; Sorescu, D. C.; Kotchey, G. P.; Star, A., Chemical Sensitivity of Graphene Edges Decorated with Metal Nanoparticles. *Nano Lett.* **2011,** *11* (6), 2342-2347.

106. Kauffman, D. R.; Sorescu, D. C.; Schofield, D. P.; Allen, B. L.; Jordan, K. D.; Star, A., Understanding the Sensor Response of Metal-Decorated Carbon Nanotubes. *Nano Lett.* **2010,** *10* (3), 958-963.

107. Mubeen, S.; Zhang, T.; Chartuprayoon, N.; Rheem, Y.; Mulchandani, A.; Myung, N. V.; Deshusses, M. A., Sensitive detection of H2S using gold nanoparticle decorated single-walled carbon nanotubes. *Anal. Chem.* **2010,** *82* (1), 250-257.

108. Ding, M.; Sorescu, D. C.; Kotchey, G. P.; Star, A., Welding of Gold Nanoparticles on Graphitic Templates for Chemical Sensing. *J. Am. Chem. Soc.* **2012,** *134* (7), 3472-3479.

109. Jung, H. Y.; Kim, Y. L.; Park, S.; Datar, A.; Lee, H. J.; Huang, J.; Somu, S.; Busnaina, A.; Jung, Y. J.; Kwon, Y. K., High-performance H2S detection by redox reactions in semiconducting carbon nanotube-based devices. *Analyst* **2013,** *138* (23), 7206-7211.